Universiteit Utrecht

Opleiding Natuur- en Sterrenkunde

Energy resolution and linearity of a pixel calorimeter prototype

Bachelor Thesis

Erik Broeils

Supervisors:
Prof Dr. T. Peitzmann
Subatomic Physics (SAP)
Dr. ing. N. van der Kolk
Subatomic Physics (SAP)

Abstract

The highly granular digital sampling electromagnetic calorimeter prototype mTower is created for R&D purposes for the proposed FoCal detector for the upgrade of ALICE. The prototype allows to test the performance of such an extremely granular detector, which will be part of the FoCal detector. In this thesis, the linearity and energy resolution of the prototype were determined. Data was collected during a weeklong test at the DESY test beam facility. It was found that the detector is linear and that the energy resolution is good, especially the constant term. The stochastic term was higher than expected, but more tests should be performed to ascertain whether that is beam or detector related.

July 17, 2020

Contents

1 Introduction

One of the major research areas of modern physics is that of Quark Gluon Plasma (QGP), the predicted state of the universe shortly after the Big Bang. This state of matter is only reached under extremely high energies or densities, which we can only achieve in special circumstances, in particle accelerators. The one that currently has the highest energies is CERN's Large Hadron Collider (LHC).

The LHC is a circular accelerator and works by accelerating and then colliding lead-ions, protons or a proton and a lead-ion. ALICE, one of the four large detectors of the LHC, is used for analysis of extreme energy densities, where QGP is most likely formed [1]. There currently an interest in the photons resulting from these collisions, as they could tell us more of what was created in these collisions. These photons can be measured when they create a shower.

A shower is a cascade of particles created by a particle entering a dense material, where it interacts with nuclei present. The initial particle loses energy from these interactions and created new particles. All these particles together are called the shower, which contains information on the initial particle.

Currently, the ALICE detector has low granularity, which is sufficient for measurements of single particles, but in extreme energy density states from before the forming of QGP, called Color Glass Condensate (CGC), these collisions generate high particle density and overlapping showers and information about the composition of these showers is lost. Therefore, a very high granularity detector is needed in addition.

This thesis will look into such a proposed upgrade for the ALICE detector, called the Forward Calorimeter (FoCal). The mTower, a prototype digital sampling calorimeter, is constructed as part of the R&D effort for FoCal. FoCal focusses on detection of direct photons emitted from these high energy collisions, which contain information of the initial state of matter at the collision. FoCal should provide a better understanding of matter at high densities.

The mTower prototype is based on a silicon-Tungsten sandwich structure made up of Monolithic Active Pixel Sensors (MAPS). In this design, the silicon layers are made up of the MAPS, small pixels of about 30 µm, that generate a signal if enough electric charge is generated to be above a certain threshold by the passing of a particle. This defines a hit in a pixel. This way, the energy of a particle is determined by the number of activated pixels, not by the energy deposited by the particle.

Because of the small size of the pixels even a modest calorimeter with a width of about 1.5 Moliere radii, such as the mTower prototype, will already have ~24 million pixels, allowing for a very

precise measurement of the energy of the particle and its shower. Furthermore, the high granularity will make it possible to separate two showers close together and analyse the shower shapes.

For my research, I participated in a week of data taking at the DESY test beam facility in Germany with the mTower prototype. With this data I determined how precise the prototype is, in particular if it is linear in the energy of the incoming particles, and its energy resolution.

2 Theoretical Background

The theory in this section largely follows C. W. Fabjan and F. Gianotti [2] and a presentation by D. Cockerill [3]. Other single references will be added when needed.

2.1 Electromagnetic Showers

When particles enter a material, they lose an amount of their initial energy by interacting with the material, specifically the atoms in the material. How this energy is lost depends on several things, but most importantly and significantly on the type of particle and the amount of energy it has. Here the focus lies on electrons/positrons and photons. They both have several ways of interacting. For both of these types of particles, we can divide two main regimes where different methods of interaction dominate. These two regimes are below and above ~10 MeV. For photons, there are 3 main ways of losing energy in a material, which are shown in Figure 1.

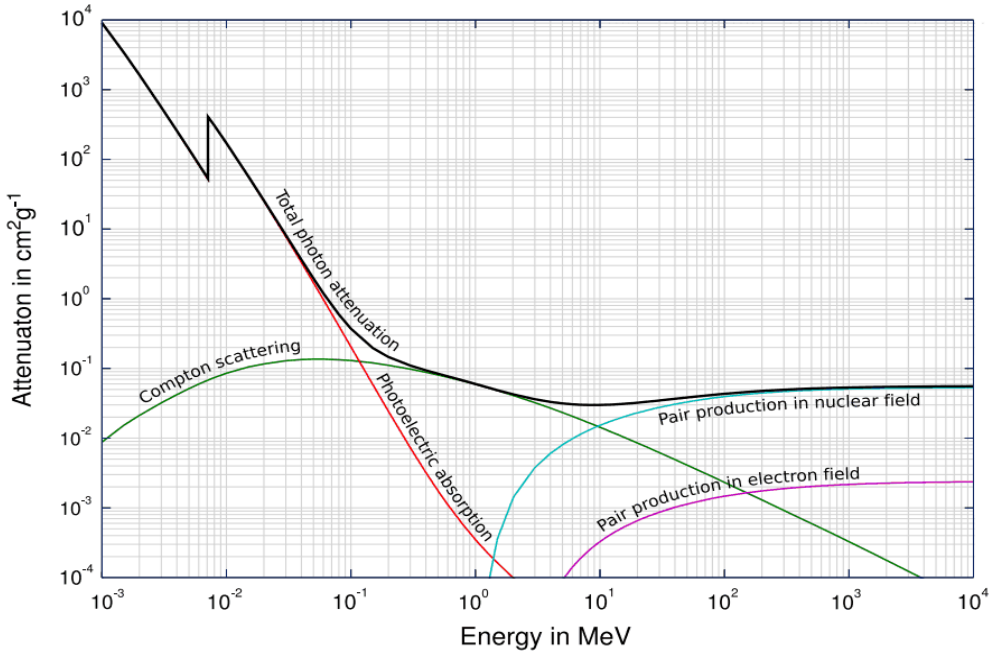

Figure 1: A cross-section of photon interaction at different energy levels. The y-axis is the attenuation, or gradual loss of flux intensity through a material. This is plotted against the energy of the photon [12].

1. The photo-electric effect. This happens at the lowest photon energies. The photon is fully absorbed by an electron and its energy is larger than the electron binding energy, which causes the electron to be ejected from the material.
2. Compton scattering. A photon has high enough energy to not be fully absorbed when it hits a bound electron, instead freeing the electron from the atom while the photon scatters in a different direction.
3. Pair production. This method begins to dominate at energies higher than around 10 MeV. When the photon is close to an atomic nucleus, it will be converted into an electron-positron pair, with the photon energy partially turning in the masses of these particles by Einstein's equation and partially into the kinetic energy of the particles. The combined rest mass of these two particles must be lower than the initial energy of the photon, while the total energy of the electron/positron pair is equivalent to the energy of the photon due to conservation of energy.

For electrons, the fractional energy loss in lead is shown in Figure 2.

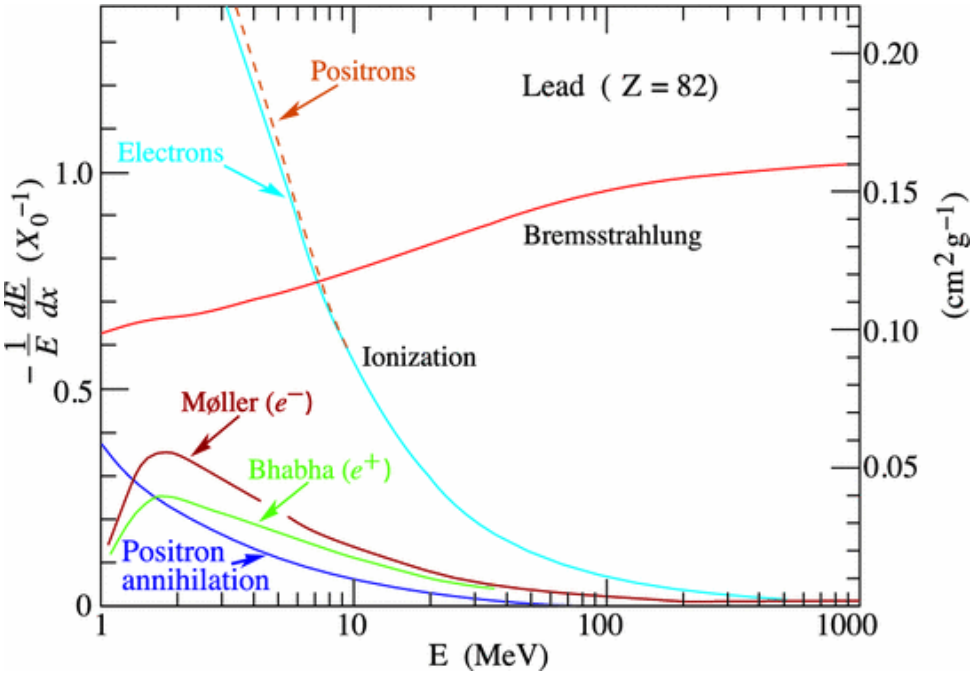

Figure 2: Fractional energy loss of electrons as a function of the energy of the particle [5].

As can be seen in the figure there are two major ways of losing energy.

1. Ionization, where the electron collides with an atomic nucleus and releases an electron from its shell. This occurs only at low energies.
2. Bremsstrahlung. This is the dominant effect at higher energies. The charged particle loses some of its kinetic energy by colliding with other charged particles in the material. It gets deflected, which causes it to lose some kinetic energy by emitting radiation in the form of a photon.

At the energies present in a high energy particle collider, >1 GeV, charged particles will produce secondary photons by bremsstrahlung and photons will produce secondary electrons and positrons by pair production. These secondary particles will then produce more particles in the same way, forming a cascade or shower of particles with lower and lower energy. This will keep occurring until the energy of the particles in the shower fall below a point called the critical energy E_c. This is around ~10 MeV. At this point bremsstrahlung and pair production are no longer the main contribution to the energy loss of the particles.

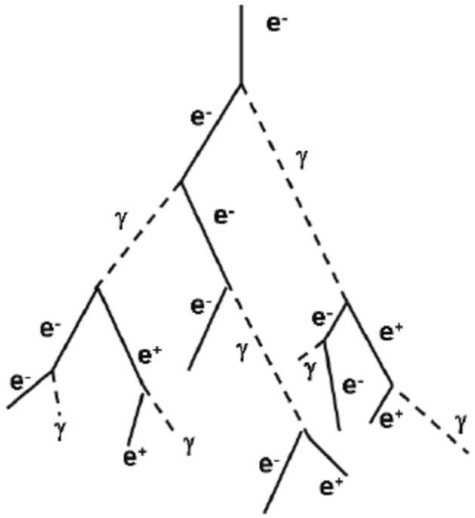

Figure 3: Simple model of an electromagnetic shower [4].

Figure 3 shows a simple model of an electromagnetic shower. At the top, we see the start of the shower, where a single particle, in this case an electron, enters a material. In this simple model, each particle will have one interaction per predefined length, called the radiation length X_0. The radiation length is defined as the average length the electron travels before having reduced its energy to 1/e of the original energy E_0 and is dependent on the material. When the particle enters the material, we see it starts to lose energy by Bremsstrahlung and produces a photon. The photon undergoes pair production and becomes a positron and electron again and this continues until the energy of the particles reaches the aforementioned critical energy. This part is called the shower maximum. After this point, there is a decrease in the number of particles in the shower and electrons/positrons and photons are stopped and absorbed by the material due to the other processes that occur at lower energies, like ionization for electrons and the photo-electric effect for photons.

Electromagnetic showers can be described by their longitudinal and transverse developments, the length and width of the shower. Both are defined by only one parameter, the radiation length, which depends completely on the material in which the shower takes place and is given by

$$X_0(g/cm^2) \cong \frac{716\ g\ cm^{-2} A}{Z(Z+1)\ln(287/\sqrt{Z})}. \quad (1)$$

Here Z is the atomic number and A the mass number of the material. For electrons and positrons, the radiation length is the average distance the particle must travel to lose (1-1/e) of its original energy, given by

$$\langle E(x)\rangle = E_0 e^{-\frac{x}{X_0}}. (2)$$

Photons are absorbed through pair production, and 9/7 X_0 is the mean free path of pair production, the average distance before the intensity of a photon beam is reduced to 1/e of the original intensity I_0 by

$$\langle I(x)\rangle = I_0 e^{-\frac{7x}{9X_0}}. (3)$$

The critical energy is defined in two different ways. Its first definition is the energy at which the energy loss caused by Bremsstrahlung and electron ionization are equal. The second definition (Rossi, 1952) is the energy where electron ionization loss per radiation length is equal to the electron's own energy E. Both are equivalent and shown below.

$$\frac{dE}{dx}(bremsstrahlung) \cong \frac{E}{X_0} = \frac{dE}{dx}(ionization). (4)$$

By using the radiation length, electromagnetic showers can be described independently of the material. To help with that we introduce the parameter $t = \frac{x}{X_0}$, the distance into the material per radiation length. With this the mean longitudinal profile of the energy is described by the following differential equation

$$\frac{dE}{dt} = E_0 b \frac{(bt)^{a-1} e^{-bt}}{\Gamma(a)}. (5)$$

Here a and b are dimensionless fit parameters depending on the incident particle (electron/positron or photon), while Γ is the gamma-function. From this equation, the position of the shower maximum can be calculated and is given by

$$t_{max} \cong \ln\frac{E_0}{E_c} + t_0 \ (6)$$

where t_0 is -0.5 for electrons/positrons and 0.5 for photons.

The above equation also shows that the shower length has a logarithmic dependence on the incident particle energy, as shown in the Figure 4. This enables a compact detector.

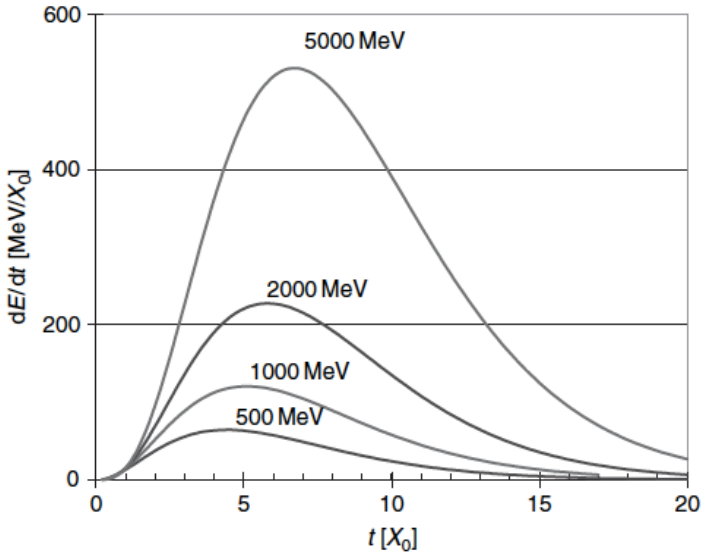

Figure 4: Longitudinal profile of electromagnetic showers for different initial energies of electrons created from a simulation [5].

To contain around 99% of the shower a material has to be about 25 radiation lengths long.

The transverse development of the shower is caused by electrons and positrons scattering in a direction other than the main shower axis. The transverse size of the shower is characterized by the Molière radius (R_M), which is proportional to the radiation length.

$$R_M(g/cm^2) \cong 21\ MeV \frac{X_0}{E_c}. (7)$$

A cylinder with a radius of one R_M and the same axis as the shower contains about 90% of the shower energy, 95% is contained in a cylinder of two R_M. Since both the radiation length and the Molière radius of most materials used in calorimeters is small, in the order of centimeters, calorimeters can be made very compact as well. This is done by selecting a material for the detector that has a small radiation length and Moliere radius.

2.2 Calorimetry

Calorimeters are detectors made to measure the energy of particles, mostly electrons, photons and hadrons. It does this by fully absorbing the energy of this particle and producing a measurable signal. They are made from absorbing material like lead or tungsten, where particles entering the calorimeter produce a shower. The particles in the shower have progressively lower and lower energy the further it goes into the material until all the particles are fully absorbed and the energy of the initial particle is absorbed. The active parts of the calorimeter measure the energy that is

deposited into the active material and this in turn serves as a measurement for the initial energy of the particle. In fact, this deposited energy is proportional to the initial energy. This proportionality comes from the sampling fraction of the calorimeter. This is basically the fraction of energy absorbed by the active layer against the total energy. Since it is also the fraction of the active material over the total material, which is known, the proportionality can be calculated.

There are two main types of calorimeter, hadronic and electromagnetic. Hadronic calorimeters are optimized to measure the energy of hadrons. The hadron entering the calorimeter initiates a hadron shower. These showers are produced by strong and electromagnetic interactions. Electromagnetic calorimeters are optimized to measure the energy of electrons/positrons and photons by way of the electromagnetic showers.

There are also two ways of constructing a calorimeter, sampling and homogeneous calorimeters. Sampling calorimeters are made up of two alternating layers of material. One is a passive absorber layer made from a dense material (e.g. tungsten or lead) where the particles in the shower lose most of their energy. The other is the active detector layer. Here the signal is provided that is sent from the calorimeter. Homogeneous calorimeters consist of just one material that acts as both absorber and active detector. The prototype is a sampling electromagnetic calorimeter, so the rest of this section will be focused on that.

Sampling electromagnetic calorimeters have several important aspects. First, in contrast to several other forms of spectrometers, the energy resolution of the calorimeter improves with energy as $1/\sqrt{E_0}$. The higher the energy of the initial particle, the better the resolution. This is perfect for particle colliders where the initial particles are often at high energy.

Another important aspect of this type of calorimeter is that their response is linear versus energy. The average signal from the active detector layers per unit of deposited energy is called the response of the detector. For electromagnetic calorimeters the response is constant, the average signal divided by the energy is the same, so the signal is linear to the energy as $S \propto E_0$. All the absorbed energy of the initial particle occurring in the shower is due to the ionization and excitation of the absorber material. To further elaborate on this, look at the total track length of the shower T_0. This is defined as the sum of all ionization tracks due to all charged particles in the cascade. Since it contains all the ionization tracks it contains all the energy the initial particle has lost in the shower.

$$T_0(g/cm^2) \propto X_0 \frac{E_0}{E_c} \quad (8)$$

This shows that the signal of all the ionization tracks is proportional to the energy of the original particle.

The final aspect of electromagnetic calorimeters is the energy resolution. This is the ability of the detector to accurately determine the energy of the incoming particle. As previously said, it improves with energy. The relative energy resolution of a realistic calorimeter is given as

$$\frac{\sigma}{E} = \frac{a}{\sqrt{E}} \oplus \frac{b}{E} \oplus c \quad (9)$$

where '$\oplus$' indicates the quadratic sum. The three contribution terms on the right-hand side are the stochastic term a, the noise term b and the constant term c.

1. The stochastic term comes from stochastic processes in the development of the shower. It is caused by fluctuations in the number of signal generating processes, the number of particles generated in the shower and quantum fluctuations in the signals. It is higher for sampling calorimeters since there are also sampling fluctuations caused by the alternating layers. Typically, the effect of this term for sampling calorimeters is about 5-20%.
2. The noise term is caused by noise in the readout electronics of the calorimeter and pile-up of more than one particle entering the calorimeter during a single measurement. This term is decreased as the energy of the initial particle increases, so for high energy particle situations, like in most colliders, this term is not very important.
3. The last term is the constant term. The contributions to this term do not depend on the energy. Imperfections in the construction or calibration of the calorimeter contribute to this term. Another part is energy from the particle lost in dead material, either in the detector or before, where it loses some energy and is no longer at E_0. At high energy it is crucial to have this term as low as possible, below 1% at least, because at high energy this term dominates.

2.3 ALICE & FoCal

The ALICE detector in the LHC measures heavy-ion and proton collisions. The goal is to study two new phenomena that exist in these conditions, quark-gluon plasma (QGP) and colour glass condensate (CGC). Both states can only be created in extremely high temperatures or pressures, like those that occurred just after the big bang or in the core of neutron stars.

QGP is the main state that is currently being studied at ALICE. It is a state of dense, hot quarks and gluons not confined in hadrons that act as quasi-free particles. It is believed to be the state of the universe in the first few microseconds after the Big Bang. This state can be replicated on a small scale in the LHC with the heavy-ion collisions. One of the current open questions is the make-up of the components, the partons, of the protons and nuclei participating in the collision. They are made of quarks and gluons, but their number is not static and depends on the circumstances of the measurement, mostly the momentum transfer Q of the process. What is found is that for larger Q, more quarks and gluons are found. Each of them has a smaller fraction x of the total momentum of the initial proton or nucleus. The density of the quarks and gluons will increase for large Q and small x, ultimately diverging. Under these conditions gluons would be the dominating parton.

A new theory states that at some point the density of the gluon peaks and doesn't increase anymore. The state would contain so many gluons that it can be described as a classical system. This is called the CGC and describes the state of the nuclei at the moment of collision, before the QGP is formed.

To more accurately study the conditions for CGC, FoCal was proposed. The FoCal detector will study photons that come directly from the interaction region, called direct or forward photons. By measuring the energy of these photons, one can gain information on the existence and make-up of the CGC. However, in this frame there are also other photons present. Most photons will come from the decay of neutral pions, the most produced particle in collisions. They decay into two photons that will be very close together. To look at the showers they produce separately and recognize that there are two showers, FoCal will have high granularity parts. These high granularity parts are being tested in the mTower prototype.

3 Hardware

3.1 mTower Prototype

The mTower is a digital sampling electromagnetic calorimeter prototype. It uses silicon pixel detectors in the active layers, giving it an extremely high spatial resolution. It has been built to test the performance of such a pixel calorimeter. The prototype, together with the previous version, are unique, there are no other high granularity sampling calorimeters. High granularity means that it has a high precision in measuring the location of particles and this makes it possible to apply two particle shower separation and do a comprehensive analysis on the electromagnetic shower shape [6]. The final FoCal design will consist of alternating layers of high granularity pixel layers and multiple low granularity silicon pad layers. Figure 5.2 shows a schematic layout of the mTower with direction from where particles enter shown, and figure 5.1 shows how it looks.

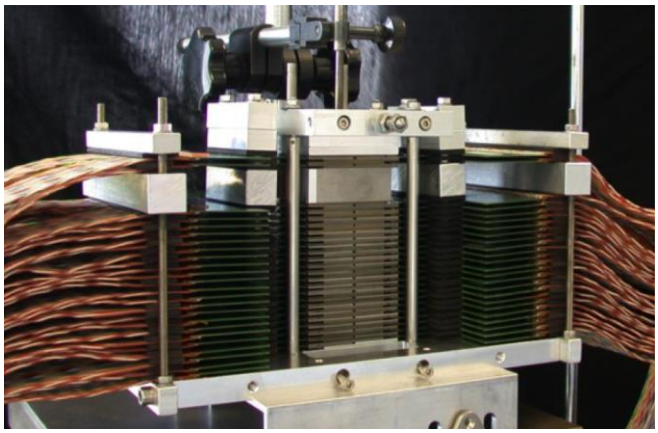

Figure 5.1: The mTower prototype [6].

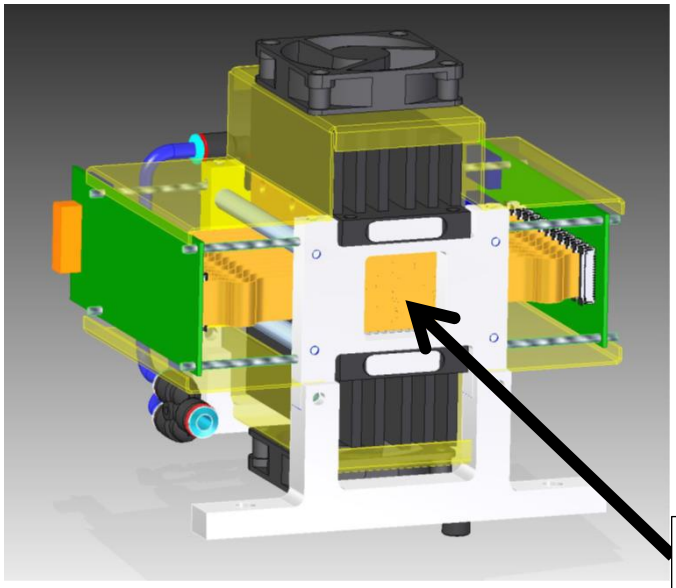

Figure 5.2: The mTower prototype [7].

The mTower is made up of 24 layers of two pixel sensors per layer. Each layer is 3.5mm thick and consists of a 3mm thick tungsten absorber and sensors. The radiation length per layer is 3.504mm. The other 0.5mm is made up of ultra-thin cables, some air and the active silicon sensors that send the signal. The Moliere radius is small, close to that of tungsten (9.327mm), because the prototype is very compact. Each layer has a sensitive surface of 30 x 30 mm^2 and consist of two sensors. Each sensor contains 1024x512 pixels, so a total of ~1 million pixels per layer [7]. Figure 6 shows the components of one layer. From top to bottom it shows the flex and chip cables that transfer data, the ALPIDE chip, the small air space and finally the tungsten absorber.

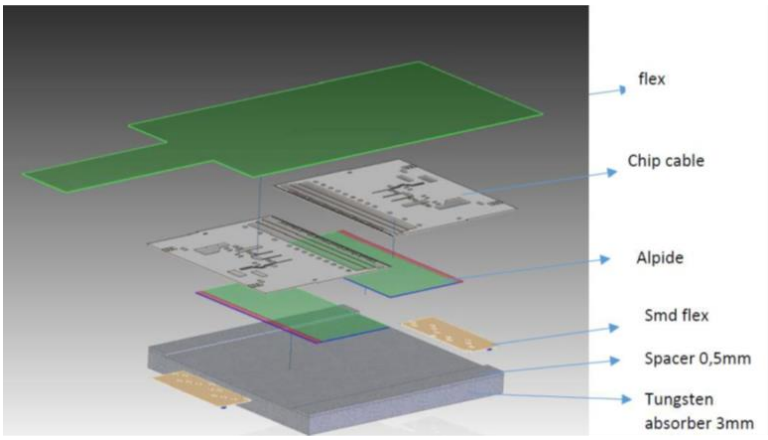

Figure 6: The cross-section of one layer [7].

3.2 ALPIDE Chips

The sensor chips used in the prototype are called ALPIDE chips [8]. They are Monolithic Active Pixel Sensors (MAPS). They are based on a CMOS imaging process, with a series of transistors that make up the in-pixel circuitry. A signal is created through charge accumulation on a diode via charge diffusion. They basically consist of three parts, a p-type substrate followed by a p-type highly doped epitaxial layer and finally the pixel circuitry (transistors and a charge collection diode). Charged particles in the shower that go through this sensor create electron-hole pairs in the epitaxial layer and charge travels to the diode via diffusion. If enough charge is accumulated at the diode it sends a signal to tell a particle passed through the pixel [9]. Figure 7 shows the layout of an ALPIDE sensor.

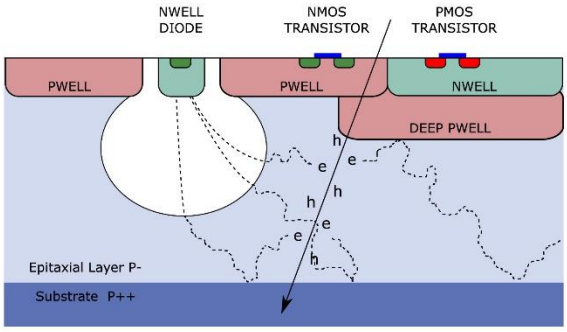

Figure 7: Layout of an ALPIDE sensor [8].

When a particle passes through the ALPIDE and the charge in a pixel exceeds the threshold energy of that pixel, it will activate and send a signal. For an incoming particle to the detector, all activated pixels together show the total path and shape of the shower. This way the detector can map the shower with great precision. Furthermore, the energy of the initial particle $E_0 \propto N_{pixels}$, the number of activated pixels, so from the number of activated pixels one can calculate the initial energy of the particle. Each pixel within the chip is 29.24x26.88 μm^2. The chip has very little dead area and its active area is 29.94x13.76 mm^2.

4 Methodology

4.1 DESY Test beam

DESY stands for Deutsches Elektronen-Synchrotron and is a German national research center of high energy physics, with a test beam facility [10]. This facility was used for a weeklong testing of the mTower prototype to check how well the measuring equipment works, if there are any problems with the detector and see how good the quality of the data is. The test beam facility provides an electron particle beam with energies up to 6 GeV. For the purposes of the test electrons were used with energies between 1 and 5.8 GeV. The high and low energy electrons were harder to create, so the beam rate, the rate at which single electrons hit the prototype, was lower at those energies. 3 GeV was the peak and at this energy there was the highest chance of multiple electrons hitting the detector at once.

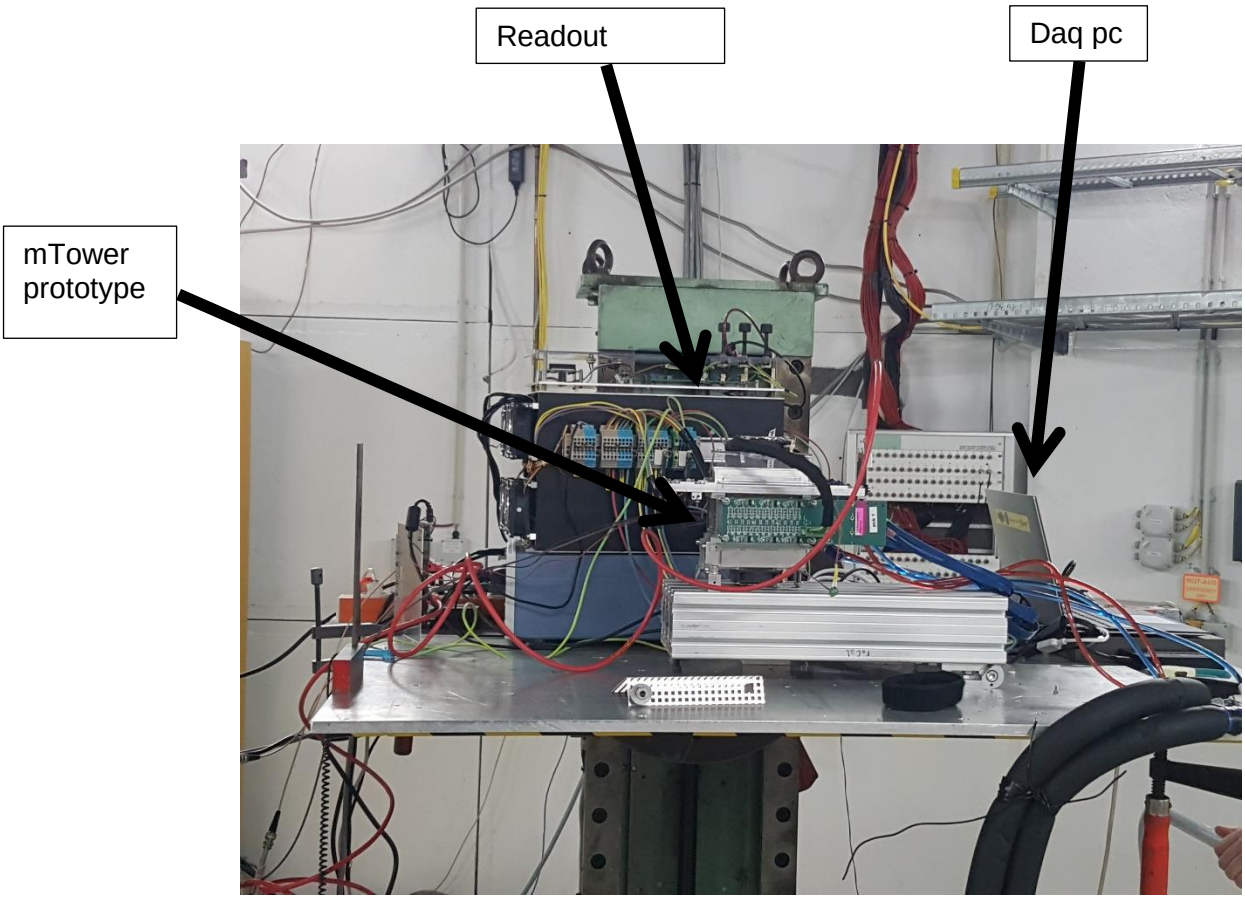

Figure 8: The prototype set-up at DESY

The mTower was put into the path of the electron beam. Figure 8 shows the set-up, with the prototype in the middle, behind that the readout boards where the data from the calorimeter is sent to. On the right is the daq pc that saves the data. Two scintillators read out by silicon photomultipliers are placed in front of the detector to help with the measurements. Each scintillator will send a signal when an electron passes through them, called the trigger signal. If both scintillators send a signal at the same time, the electron will have passed through both and will continue into the detector. At this point a trigger signal is sent to the detector and a measurement will take place for 2 µs, called an event.

Multiple measurements are taken in runs consisting of between 1500 and 3000 cycles of 100 to 500 triggers, thus each run contains in the order of 150 000 events. Two collimators are also placed in front of the detector to focus the beam on the center of the calorimeter prototype, and to reduce the beam rate.

4.2 Analysis

For the analysis of the data from the test week, a data processing and analysis framework called ROOT is used. ROOT is based on C++ and is developed at CERN, to be used in the analysis of high energy physics [11]. In the analysis, the number of hits recorded for each event is collected

in a histogram that then shows the distribution of the number of hits. An example of this is figure 9. It shows several peaks corresponding to electron showers, coloured red, blue and green corresponding to the number of electrons, respectively 1, 2 and 3.

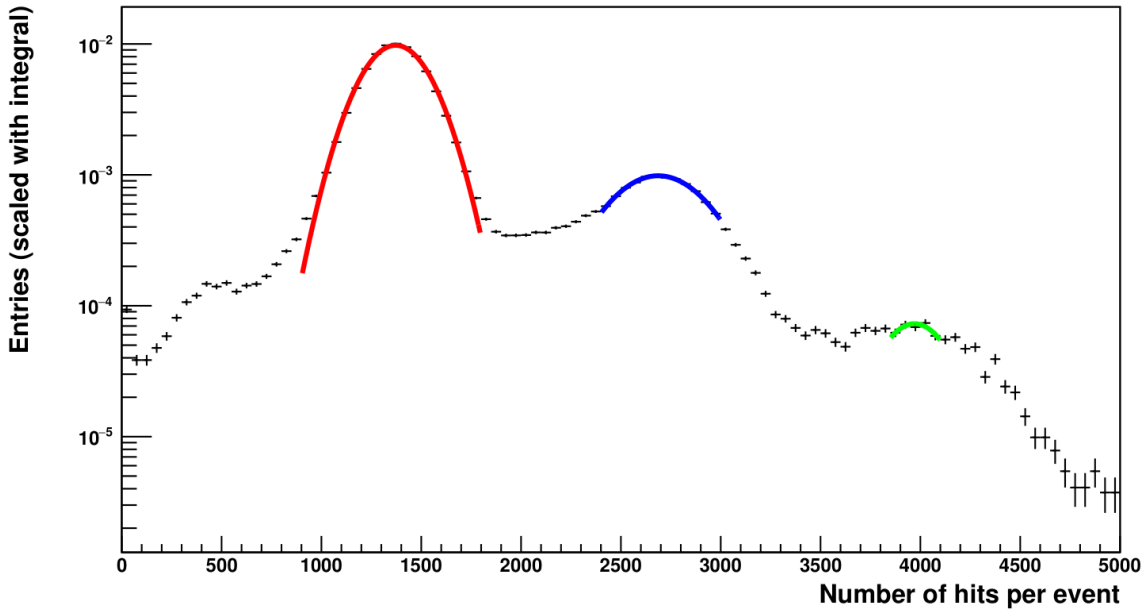

Figure 9: Histogram showing the number of hits per event.

Peaks in the histogram correspond to a full shower from one or more electrons. The first peak is the highest and corresponds to one shower and thus one initial electron entering the detector. A peak that corresponds to two electron showers will have approximately double the number of hits of a peak corresponding to one electron shower. Appendix A shows these histograms for all the runs used in the analysis with Gaussian fits for each of the peaks.

For the calculation of the linearity and energy resolution, only the events with one shower, so one electron hitting the detector, are required. The initial data, and histograms created from that data, contain background noise and partial showers that don't develop fully in the detector. Additionally, as is clear from Figure (HISTOGRAM), events with multiple electrons entering the detector at the same time (pile-up) are included. The event set needs to be cleaned up before proper results can be found. For this purpose, selection criteria, developed by A. van Bochove, were used on the data to eliminate multi-shower events and background noise. Table 1 shows the runs used for analysis per energy.

Table 1: Table of all the runs used in the analysis and which electron energy they correspond to.

Energy (GeV)	Runnumber
1	1263, 1336, 1343
2	1276, 1337, 1344
3	1262, 1335, 1341
4	1274, 1338, 1345
5	1261, 1308, 1333, 1339
5.8	1309, 1310, 1346, 1376

The cleaned-up data is then combined for each beam energy and the number of hits per event is plotted into histograms. The distributions of the number of hits are then fitted with a Gaussian. The values of the mean and sigma of these Gaussian fits are used to evaluate the linearity and calculate the energy resolution of the prototype. The results of this analysis are shown in the next chapter.

5 Results

5.1 Voltages to the ALPIDES

During the week of testing, there were three different voltages used to power the ALPIDES. Respectively 2.2, 2.3 and 2.5V. This should have no influence on the data. The PCB in between the power supply and the chips, that supplies the voltage to the chips, restricts the incoming voltage to 1.9V. To check this and see if the data from the lower and higher voltages is not significantly different, the linearity and energy resolution were compared of 2.2 and 2.5V

For the situation of lower voltage, 2.2V, the runs {1263, 1276,1262,1274, 1261} were used, whose hit distributions are shown in Appendix A. For the higher voltage, 2.5V, two sets of runs were chosen. If these two sets at 2.5V are practically the same, but the lower voltage set has a very different outcome, it will not be included in the analysis. If the two sets at 2.5V have similar deviation as the lower voltage set, than all runs can be used in the final analysis. The two sets at 2.5V were runs {1336, 1337, 1335, 1338, 1333, 1310} and runs {1343, 1344, 1341, 1345, 1339, 1346}. The results of these runs are shown in the Table 1.

Run:	Energy (GeV)	Power (V)	Mean	Uncertainty of mean	Sigma	Uncertainty of sigma
1263	1	2.2	278.1	1.7	65.1	2.7
1336	1	2.5	281.1	1.6	62.8	2.5
1343	1	2.5	281.6	1.5	64	2.4
1276	2	2.3	570.6	2.2	98.2	2.5
1337	2	2.5	560.6	1.9	89.5	2
1344	2	2.5	562.5	1.9	91	2
1262	3	2.2	838.9	3.2	112.9	2.5
1335	3	2.5	843.8	3	111.8	2.5
1341	3	2.5	844.7	1.9	113.6	1.4
1274	4	2.2	1105.6	1.9	122.7	1.9
1338	4	2.5	1108.1	2.6	125.9	2.7
1345	4	2.5	1106.7	1.7	127.1	1.7
1261	5	2.2	1378.9	1.5	143.8	1.1
1333	5	2.5	1387.6	1.9	139.3	1.4
1339	5	2.5	1386.5	1.2	144.3	0.9
1310	5.8	2.5	1580.4	2	152.7	1.7
1346	5.8	2.5	1569.6	1.3	151.3	1.1

Table 2: This table lists all the runs used for the comparison, the energy of the beam and the power to the Alpides. For each run the mean number of hits per event for a 1 electron event is listed with its uncertainty, along with the sigma of the distribution and its uncertainty. The blue runs correspond to the 2.2V set, the green and blue runs are the two 2.5V sets.

This table shows two main things. First, the mean number of events is significantly different for the lower voltages for several energies, but not for all of them. Specifically, at 2 and 5 GeV. Furthermore, there is no depence on time of the runs with the same power output to the ALPIDES, except at the 5.8 GeV energy, where we see a similar difference as for different power supply at 2 and 5 GeV.

The mean number of hits per event for lower power input shows a sizeable difference from that of higher input. At each beam energy, it is more than two standard deviations away from the two sets at 2.5V. This deviation even reaches 5 standard deviations for 2 GeV, which is also the only energy where the mean was higher for the 2.2V runs. This difference is not seen in the values of the sigma, so the spread in the number of hits for all runs of equal energy is the same.

This table also shows there is no dependence on time. The two sets of runs at equal power input are not distinct from each other. The mean number of hits for all energies are within one standard deviation. The outliers here are the measurements taken at 5.8 GeV, where there is a 5 standard deviation difference. Possibly because at this energy the test beam produces a very low number of electrons compared to other energies causing a larger statistical difference between them.

To look at how large the effect of this deviation is on the results, the linearity and energy resolution of these sets are determined. There should be a difference in the linearity for higher and lower inputs, since the mean number of hits is different for these two inputs, but not one for the energy

resolution. Figures 10, 11 and 12 show the linearity for the three sets. The p0 and p1 terms correspond to the b and a terms respectively in a standard linear equation $y = ax + b$.

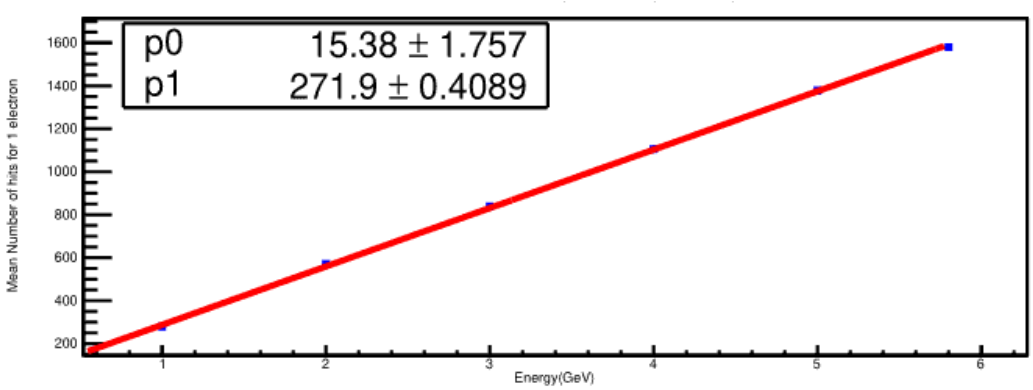

Figure 10: Mean values of the distributions of the number of hits as a function of the beam energy for a power input of 2.2V, corresponding to the blue runs in Table 2. Also shown is a fit to the data with a linear function.

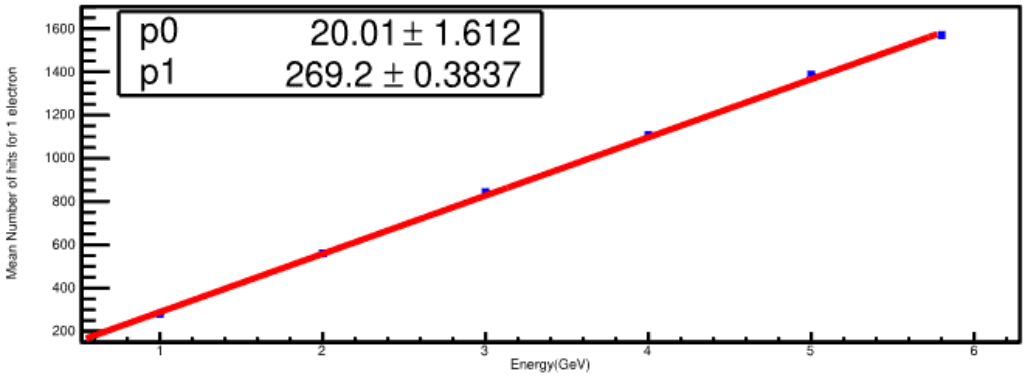

Figure 11: Mean values of the distributions of the number of hits as a function of the beam energy for a power input of 2.5V, corresponding to the red runs in Table 2. Also shown is a fit to the data with a linear function.

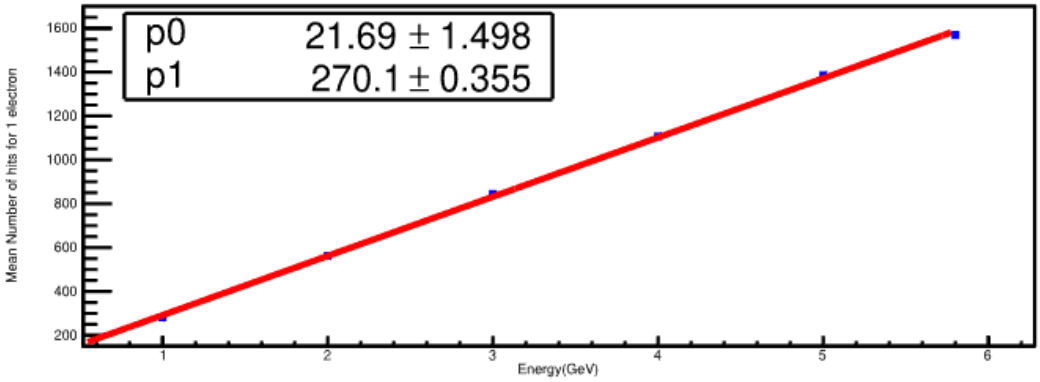

Figure 12: Mean values of the distributions of the number of hits as a function of the beam energy for a power input of 2.5V, corresponding to the green runs in Table 2. Also shown is a fit to the data with a linear function.

The linearity of the three sets does indeed show a significant difference between the lower and higher voltages, but only for the intersection, as seen in the p0 value of the three plots. The

intersection point for the lower input is over two standard deviations lower while the two sets at 2.5V are within range of each other. The slope is also higher, given by the p1 values, but the deviation there is much less significant and here the values for the two equal sets are not within one standard deviation of each other. For the slope we can conclude that the deviations are similar for all three sets and the lower power supply has no influence.

Figures 13, 14 and 15 show the energy resolution for the three sets. Here the p0 and p1 terms are constant and stochastic term respectively of the energy resolution equation (9).

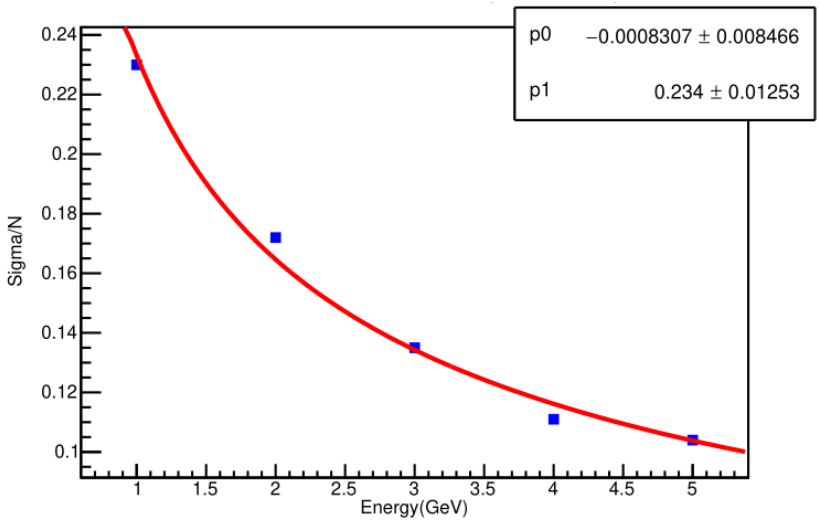

Figure 13: Plot of sigma divided by the mean values of the number of hits as a function of the energy, corresponding to the blue runs in Table 2. This was done for a power input of 2.2V.

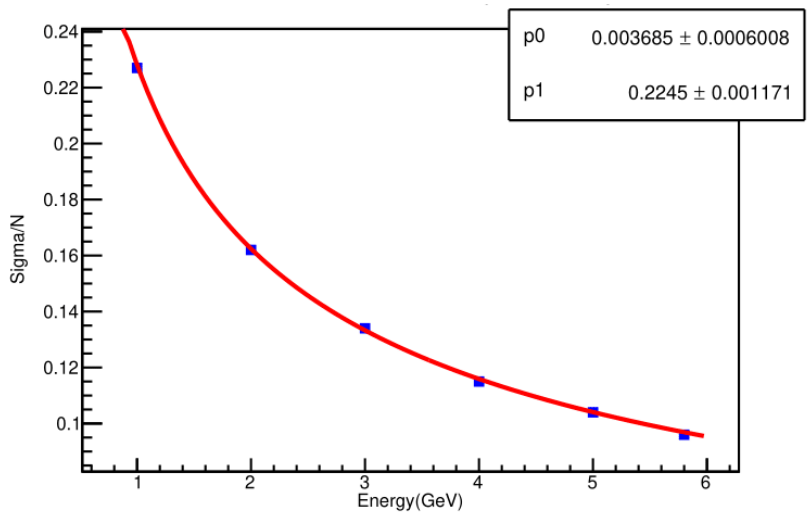

Figure 14: Plot of sigma divided by the mean values of the number of hits as a function of the energy, corresponding to the red runs in Table 2. This was done for a power input of 2.5V.

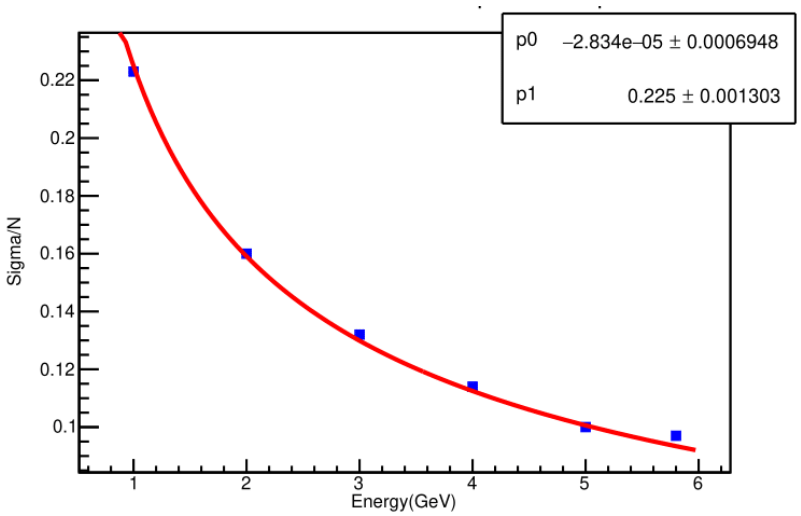

Figure 15: Plot of sigma divided by the mean values of the number of hits as a function of the energy, corresponding to the green runs in Table 2. This was done for a power input of 2.5V.

The energy resolutions of the three sets are much closer together, but there is still a difference that is not expected. The 2.5V runs show no real difference to each other, but the resolution for the lower input is slightly worse.

This comparison of the results at the two power inputs has shown there is a difference in individual values for several electron energies, but for the linearity and resolution plots this is not large enough to warrant an exclusion of this data and for the full analysis both sets of data will be used.

5.2 Combined Runs

For each energy, the data of several runs are combined. For 1, 2, 3 and 4 GeV three runs were used and for 5 and 5.8 GeV four runs were used. These were all the runs that had the selection criteria applied to them. The data of these runs was combined and put into one number of hits distribution histogram, on which the selection criteria are used. These histograms are shown in Figures 16 to 21.

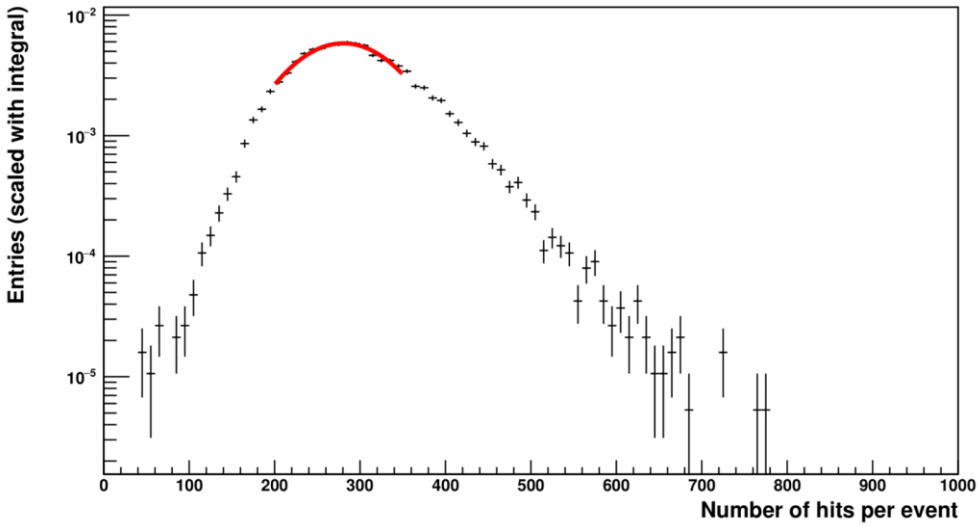

Figure 16: Distribution of the number of hits of all runs at 1 GeV combined.

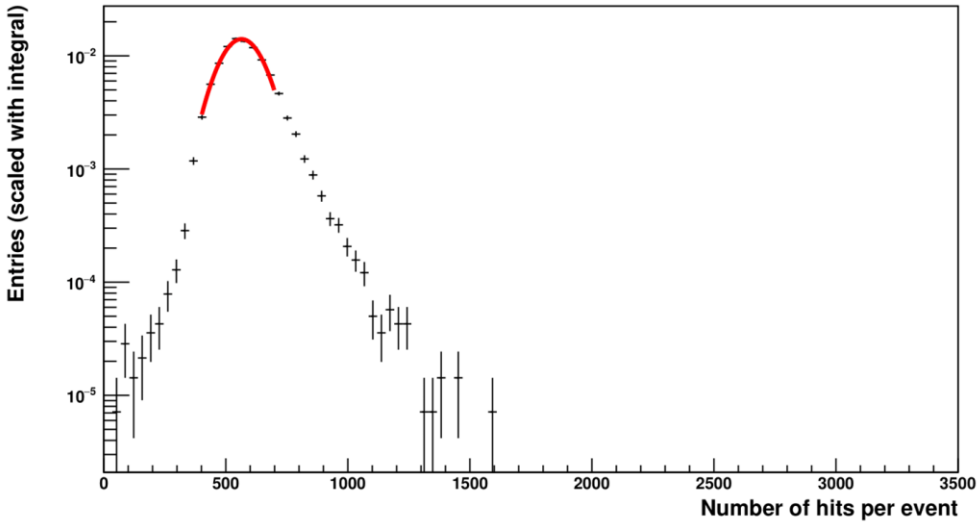

Figure 17: Distribution of the number of hits of all runs at 2 GeV combined.

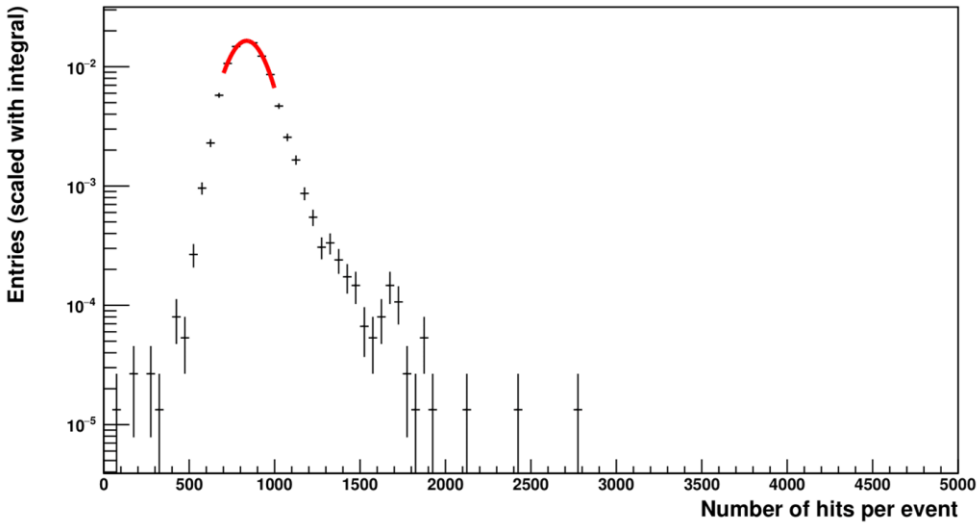

Figure 18: Distribution of the number of hits of all runs at 3 GeV combined.

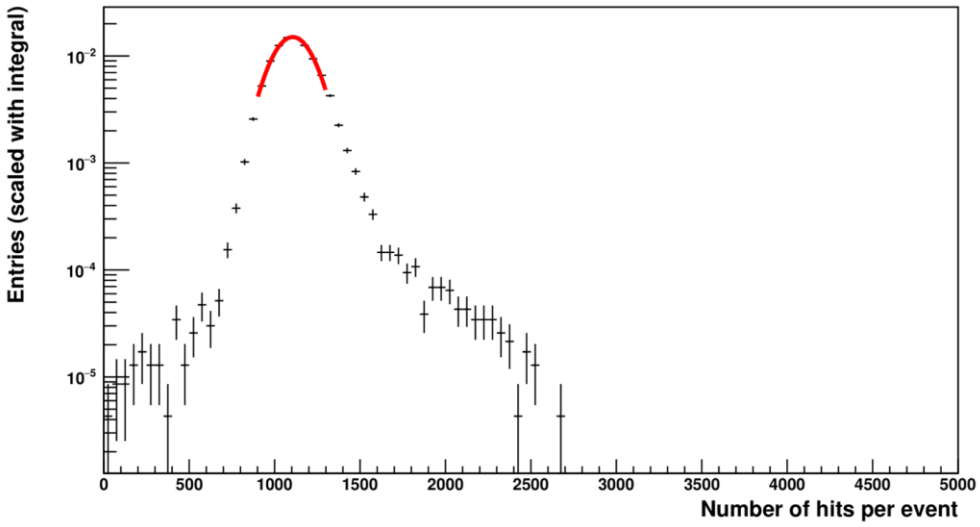

Figure 19: Distribution of the number of hits of all runs at 4 GeV combined.

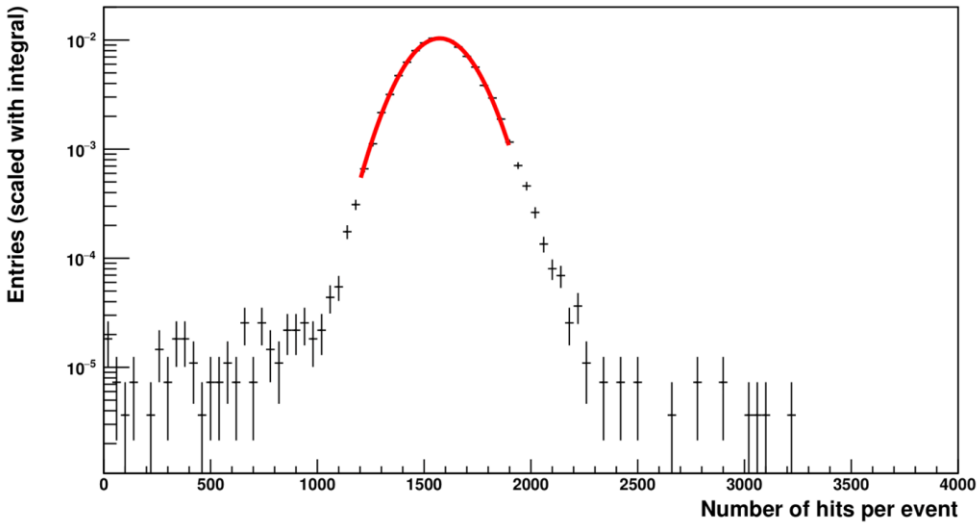

Figure 20: Distribution of the number of hits of all runs at 5 GeV combined.

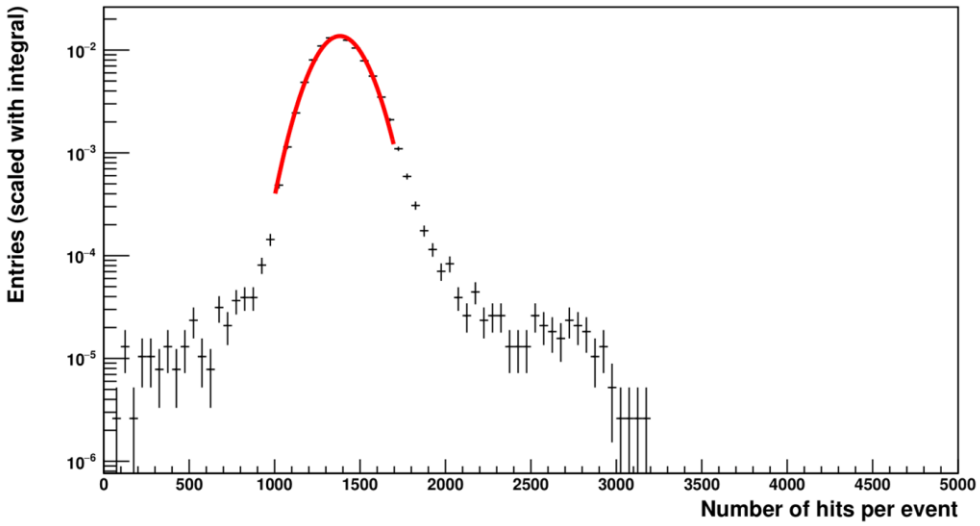

Figure 21: Distribution of the number of hits of all runs at 5.8 GeV combined.

The selection criteria have a large effect on the number of hits distribution. The peaks corresponding to multiple electron hits are gone for all energies, while the tails on both side of the one electron peak have been reduced. The resulting values from the Gaussian fit, the mean and sigma, are displayed in Table 2.

Table 3: The mean and sigma for the fits of the combined histograms for each energy and their standard deviations.

Energy (GeV)	Mean value	Standard deviation mean value	Sigma	Standard deviation sigma	Sigma/Mean
1	280.4	0.9	63.9	1.5	0.228
2	564.4	1.2	93.1	1.2	0.165
3	836	2.5	120.5	3.9	0.144
4	1105.8	1.2	127.3	1.5	0.115
5	1369.7	1.7	141.2	2.9	0.103
5.8	1573	1	152.3	0.9	0.097

5.3 Linearity

For the linearity, the mean values in the above table were plotted against the energy and fitted with a linear function, resulting in the plot in Figure 22.

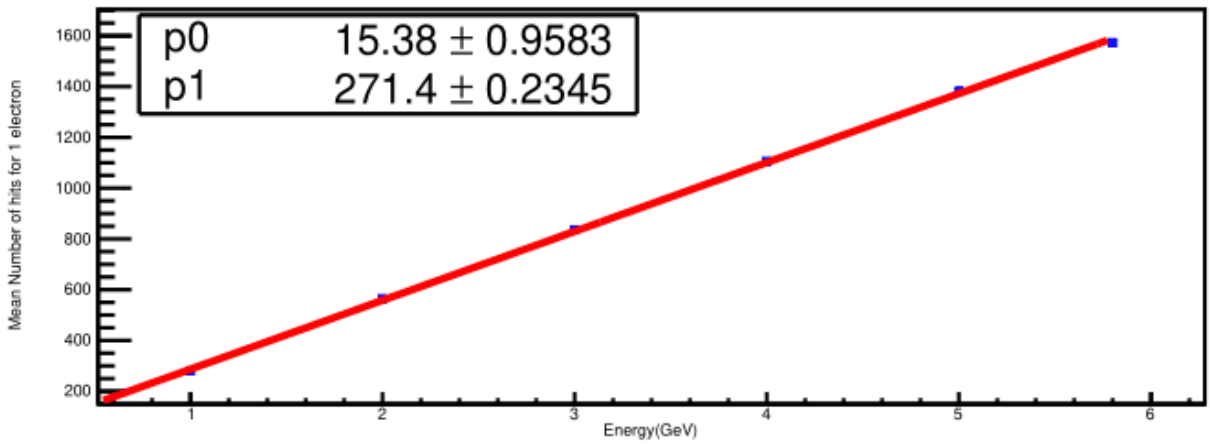

Figure 22: Mean values of the total distributions of the number of hits as a function of the beam energy. Also shown is a fit to the data with a linear function.

The response of the detector is clearly linear versus the energy, with a slope of 271.4. The reduced chi-squared test gives a result of 3.545 which is high. This can be explained by seeing that especially the 5.8 GeV mean lies below the fit and the fact that the means have a small standard deviation. At energies above 5 GeV, the test beam was at the limit and it was harder to produce a lot of electrons, meaning that value would be more uncertain.

The constant term of the linear function here is not zero. There will always be cosmic particles going through the calorimeter, or pixels that are always activated or on, no matter if they were hit or not. These hot pixels and cosmic particles are the cause of some noise in the device, which shows itself in a non-zero constant term here.

5.4 Energy Resolution

For the resolution we get the graph in figure 23.

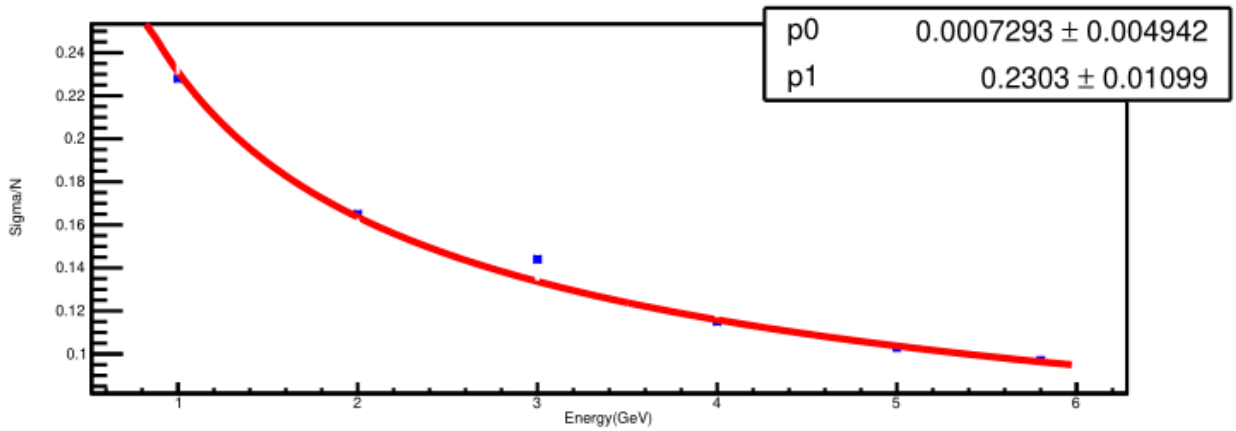

Figure 23: Sigma/N plotted against the energy and fitted with the function given in Equation (10)

The reduced chi-squared test for this fit gives a value of 0.709, which makes it a good fit. There is an outlier in the data points, 3 GeV. At this energy the test beam created the most electrons, so it had the highest higher peaks. This could also cause more pile-ups, that have not all been removed, resulting in a gaussian fit with a greater width and thus a higher sigma. A single outlier like that has little influence on the fit used. It was found that for the fitting function, just

$$\sigma/N = a + b/\sqrt{E} \quad (10)$$

was better than the full function, so the 1/E term was left out. This can be justified by reasoning that the calorimeter is used at high energies, bigger than 1 GeV. The 1/E term is then negligible.

The constant term of the fit, p0 or a, is very small. Since this term is affected by the calibration and construction of the calorimeter, the conclusion here is that the calorimeter itself is well constructed. This is also positive for high energies, where this term is the dominant one.

The stochastic term, corresponding to p1 or b, is rather high. It is usually in between 5 to 20% for analog electromagnetic sampling calorimeters. For this digital calorimeter prototype, it is 23%. A possible explanation for this could be that since the stochastic term is dominated by quantum and sampling fluctuations, the beam itself wasn't completely constant and fluctuated in the electron output. This would cause a higher value as seen here. Another explanation is that there is some statistical problem within the calorimeter. While it only measures for 2 µs at a time, afterwards it takes a few seconds to process the data. This could cause some statistical issues and in turn explain the higher value. The prototype also has a very small sampling fraction, which means there is a higher chance of stochastical differences and sampling fluctuations. Finally, this is also still a prototype and the development is not complete, while the 5 to 20% value is for well established calorimeters.

6 Conclusion & Discussion

In this thesis, I looked at the linearity and energy resolution of the mTower prototype. It was determined that the voltage coming from the power supply has no influence on the resulting measurements coming from the calorimeter. The detector is linear in the energy with a slope of 271.4 ± 0.2. The intersection of the linearity does not occur at zero, but at a slightly higher point. This is because there will always be a background noise caused by thermic noise, and the detector contains several hot pixels that are always activated.

The background thermic noise could be reduced by doing a pedestal run with the detector. Let it run for some time while not activating the particle beam, so that the thermic noise can be determined. This can then be subtracted in the histograms to get an improved data set. For the hot pixels, they could be detected by looking in the data and finding pixels that always show a hit. Then they could be ignored in the analysis.

The energy resolution of the prototype looks good. There is a very low constant term, showing that there is no internal issue in the detector, and everything is working. This is also positive for high energy situations, where this term is the dominating term. The stochastic term is rather high, above the standard 5-20%. Since this term is caused by stochastic fluctuations, one possible reason is that the beam rate in the collider was also fluctuating, decreasing the resolution of the detector.

A few improvements could be made in the current analysis. During analysis a simple Gaussian fit was used on the histograms, but they were not just simple Gaussian distributions. A more complex fit could be used that considers asymmetry of the peaks in the histogram to gain more precise values for the mean and the sigma. New selection criteria could also be looked at, that might even better eliminate the unwanted data.

These results can be used to make the current simulations of the prototype more realistic. Dead pixels that are found could be added to the simulation to improve it, just like the background noise.

References

[1] "ALICE," [Online]. Available: https://home.cern/science/experiments/alice.

[2] C. W. Fabjan and F. Gianotti, "Calorimetry for particle Physics," 2003. [Online]. Available: http://lappweb.in2p3.fr/~chefdevi/Detector_reports/Calorimetry/Fabjan.pdf.

[3] D. Cockerill, "Introduction to Calorimeters lecture," 2016. [Online]. Available: file:///C:/Users/Erik/Documents/Universiteit/Bonz2/papers/Calorimetry-lecture-to-Southampton-students-4May2016-Cockerill-compressed.pdf.

[4] P. Rocca and F. Riggi, "The Use of Avalanche Photodiodes in High Energy Electromagnetic Calorimetry.," in *Advances in Photodiodes*, 2011, p. 251.

[5] Masciocchi, "Electromagnetic calorimeters lecture," 2017. [Online]. Available: https://www.physi.uni-heidelberg.de/~sma/teaching/ParticleDetectors2/sma_ElectromagneticCalorimeters.pdf.

[6] A. d. Haas, G. Nooren and T. Peitzmann, "The FoCal prototype – an extremely fine-grained electromagnetic calorimeter using CMOS pixel sensors," 2017. [Online]. Available: https://arxiv.org/abs/1708.05164.

[7] N. van der Kolk, "FoCal a highly granular digital calorimeter," 2019.

[8] M. Mager, "ALPIDE, the monolithic Active Pixel Sensor for the ALICE ITS upgrade.," *Nuclear Instruments and Methods in Physics Research Section A: Accelerators, Spectrometers, Detectors and Associated Equipment,* pp. 434-438, 11 July 2016.

[9] W. Snoeys, "CMOS monolithic active pixel sensors for high energy physics," *Nuclear Instruments and Methods in Physics Research Section A: Accelerators, Spectrometers, Detectors and Associated Equipment,* pp. 167-171, 21 November 2014.

[10] "DESY," [Online]. Available: https://www.desy.de/.

[11] "ROOT," [Online]. Available: https://root.cern/about/.

[12] N. Connor, "What is Interaction of Gamma Radiation with Matter - Definition," 2019. [Online]. Available: https://www.radiation-dosimetry.org/what-is-interaction-of-gamma-radiation-with-matter-definition/.

[13] F. Kuger, "Signal Formation Processes in Micromegas Detectors and Quality Control for large size Detector Construction for the ATLAS New Small Wheel.," 2017. [Online]. Available: https://arxiv.org/abs/1708.01624.

A Appendix

A.1 Number of hits Distributions of individual runs

Below are the histograms of the number of hits distribution for all the individual runs that were used in the analysis for the power supply, before the selection criteria were applied. Here the colours of the individual fits correspond to the number of electrons causing that peak. In order of electrons causing the peak they are red, blue, green and yellow corresponding to one, two, three and four electrons.

1 GeV runs

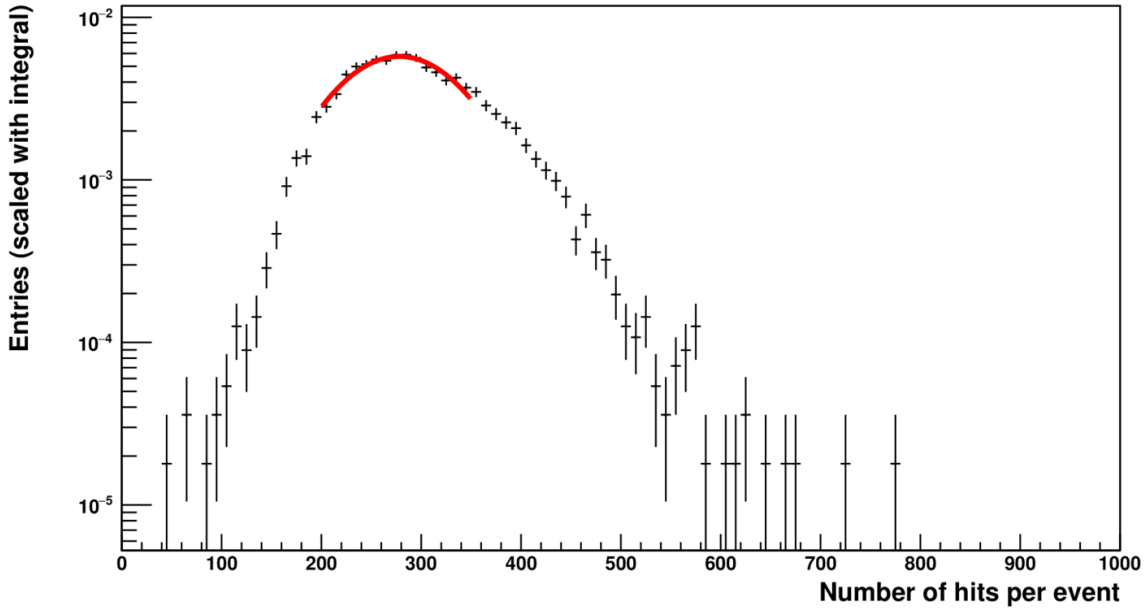

Figure 24: Run 1263

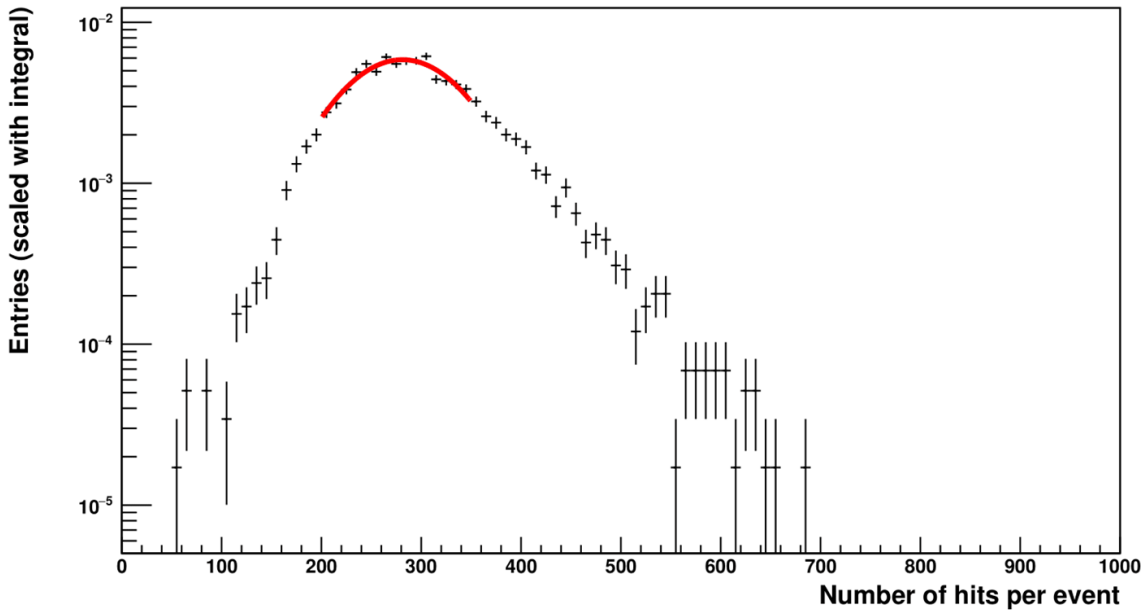

Figure 25: Run 1336

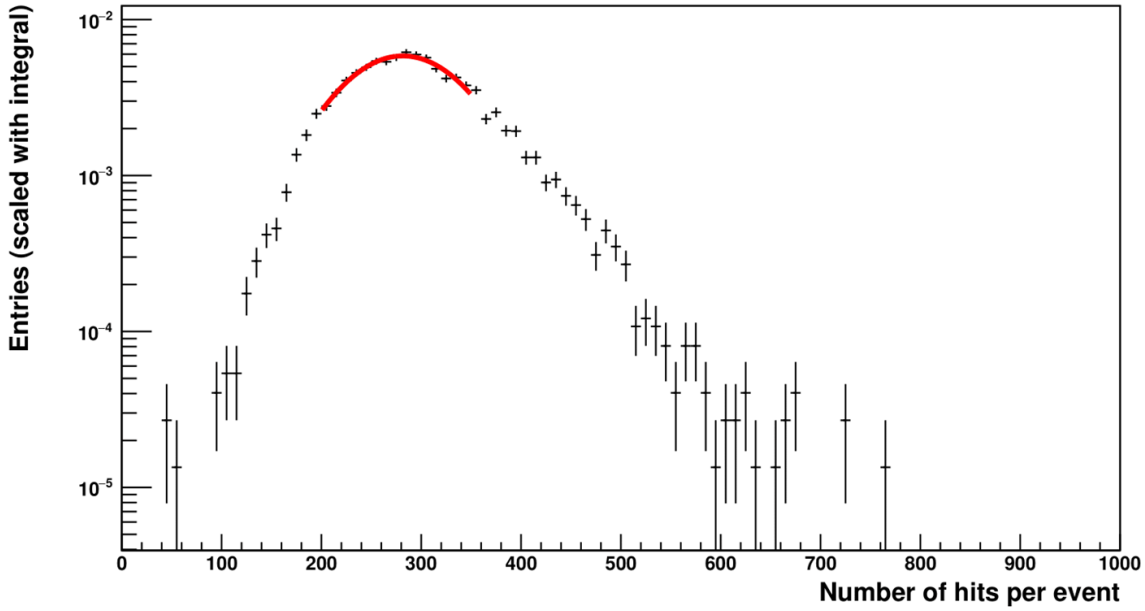

Figure 26: Run 1343

2 GeV runs

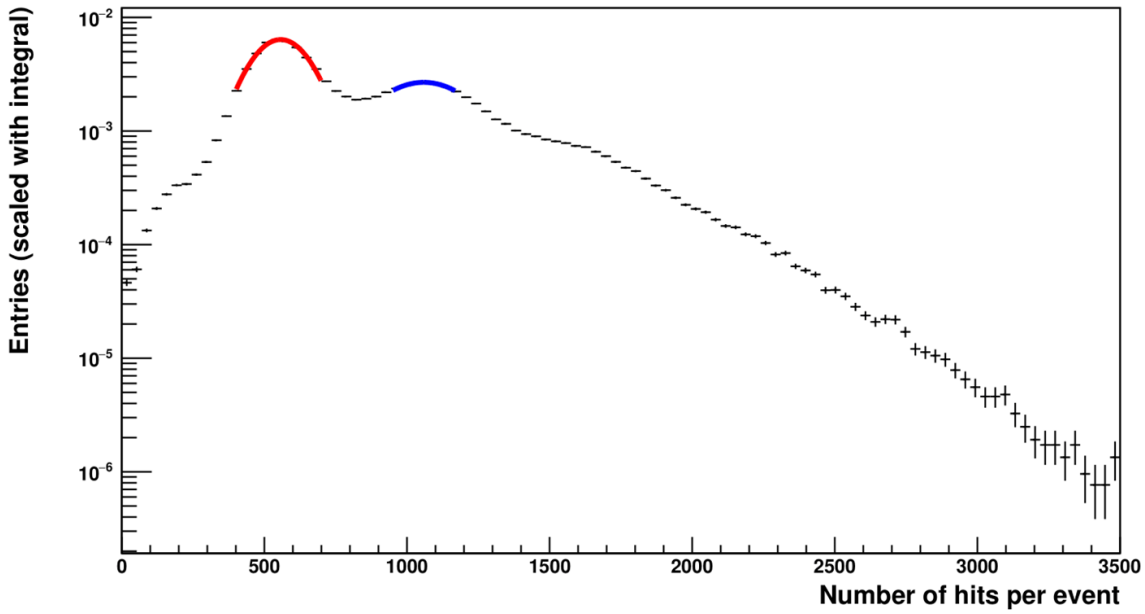

Figure 27: Run 1276

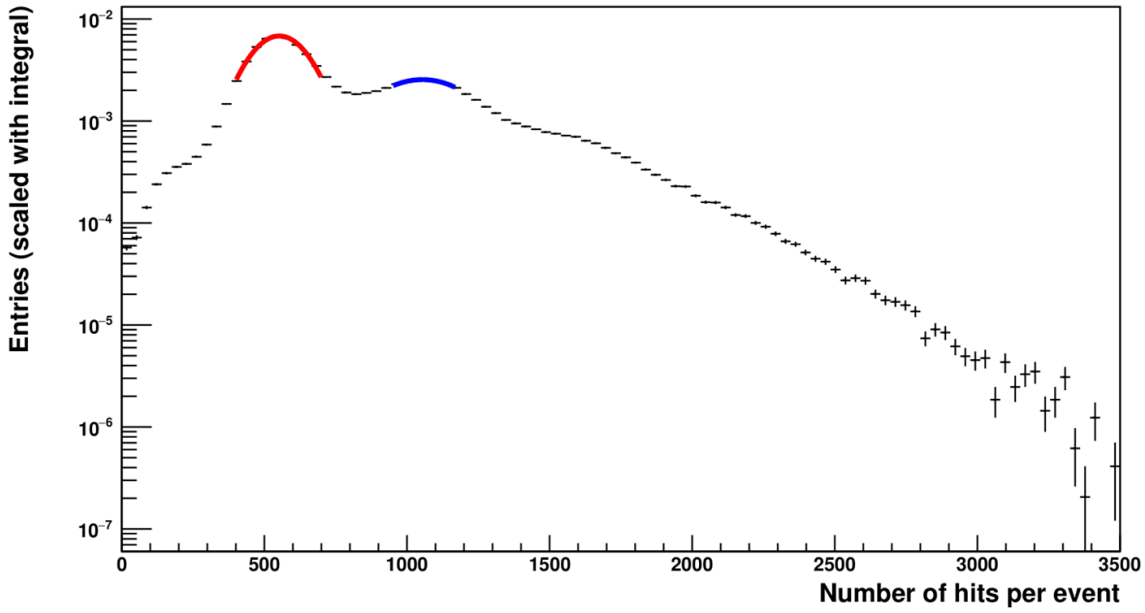

Figure 28: Run 1337

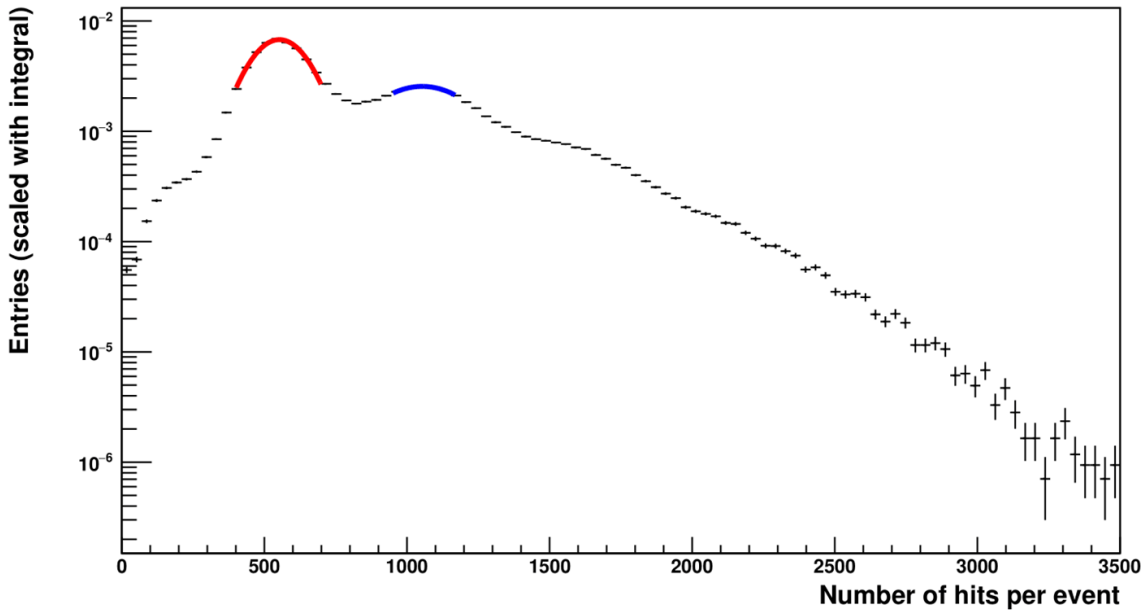

Figure 29: Run 1344

3 GeV runs

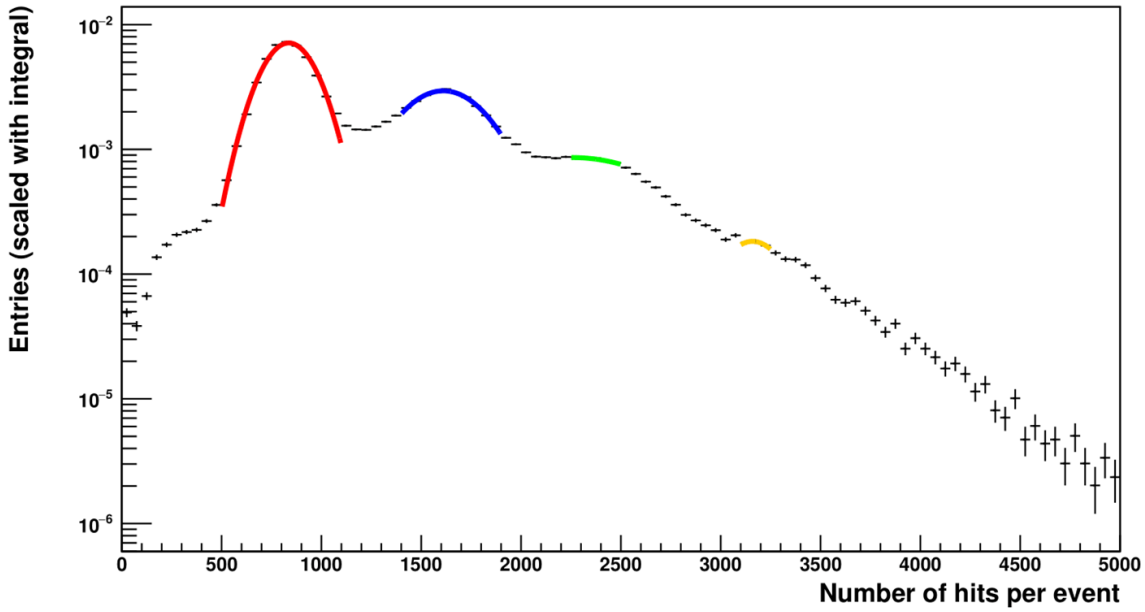

Figure 30: Run 1262

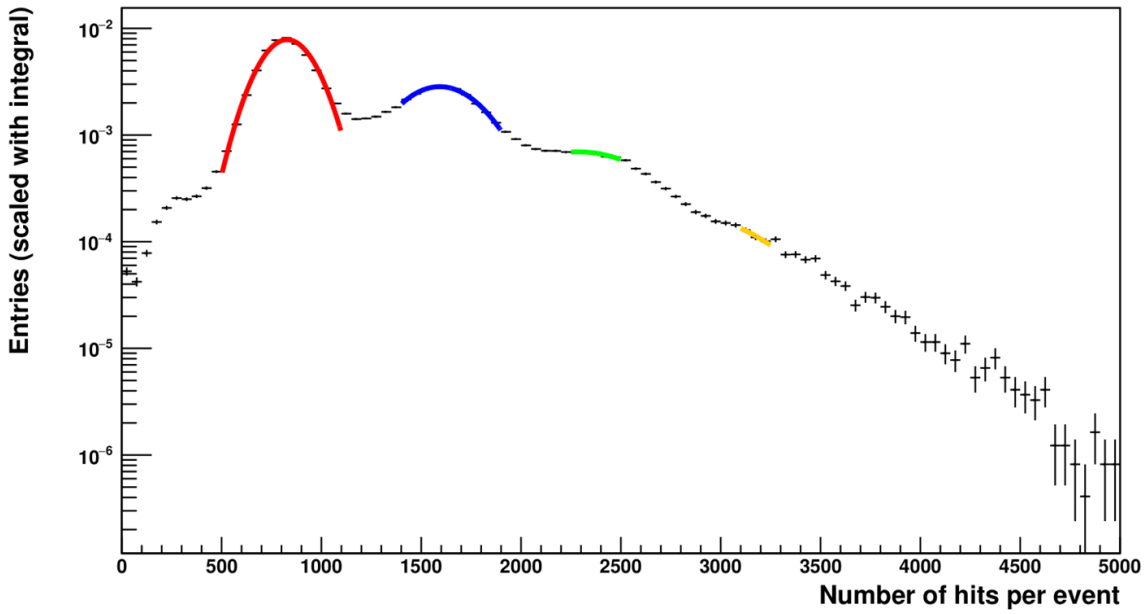

Figure 31: Run 1335

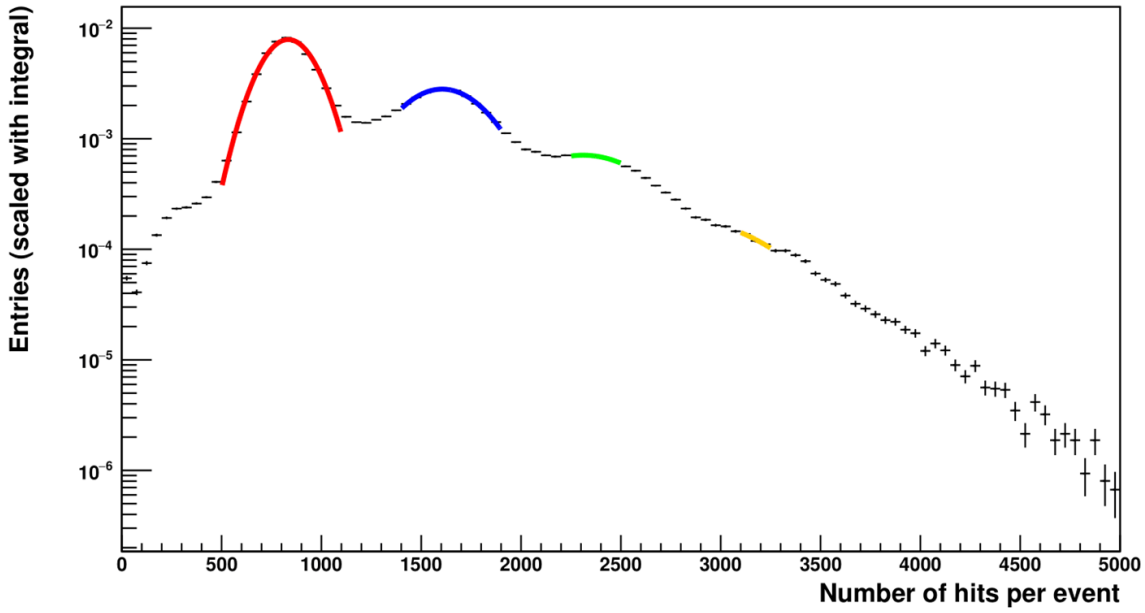

Figure 32: Run 1341

4 GeV runs

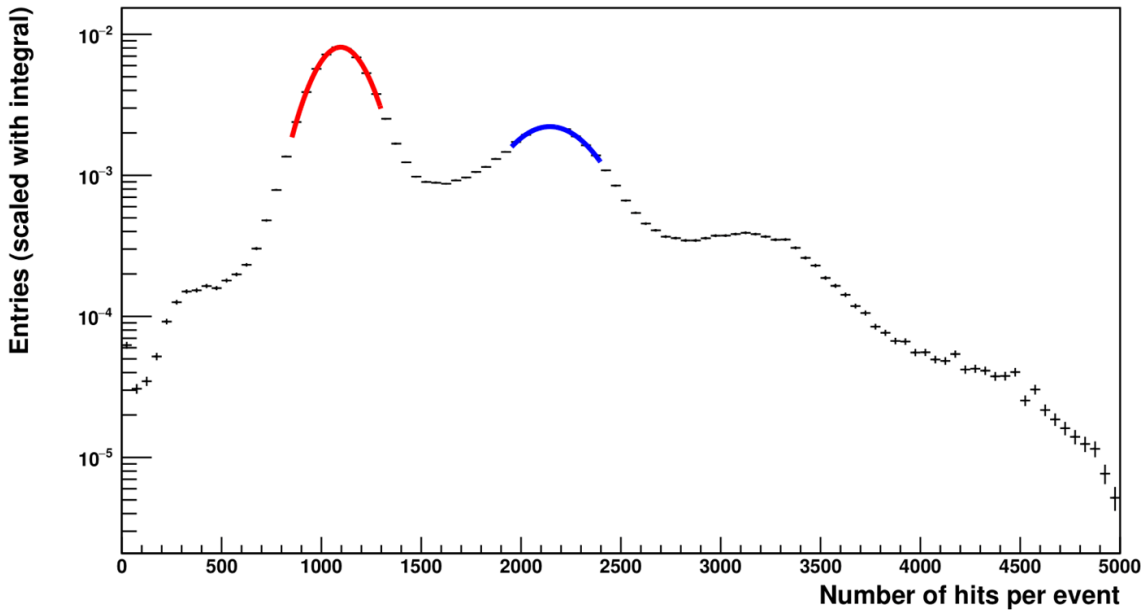

Figure 33: Run 1274

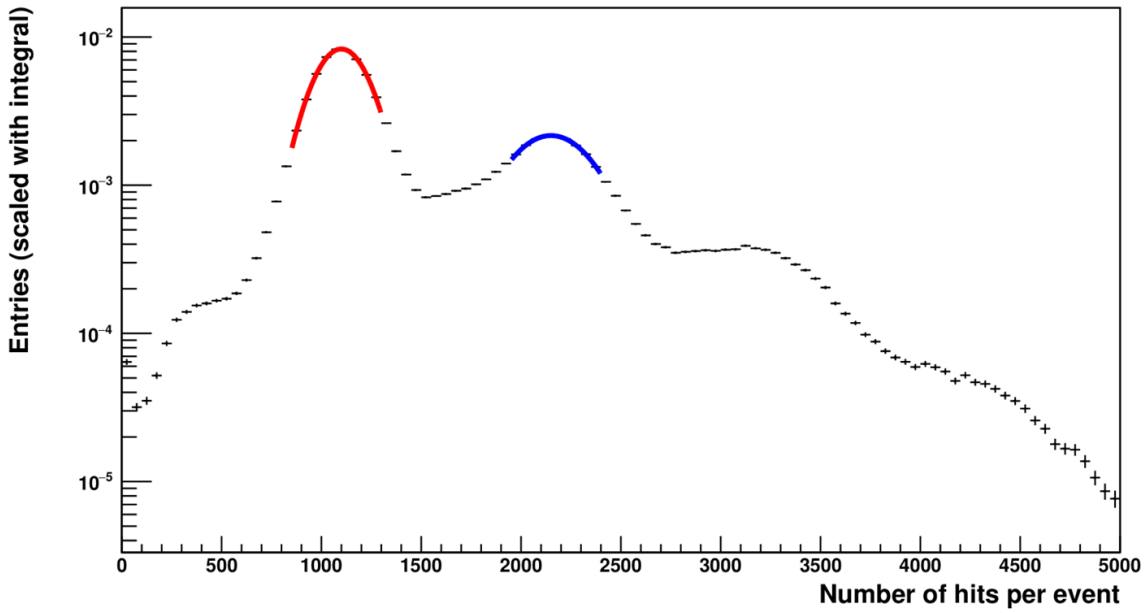

Figure 34: Run 1338

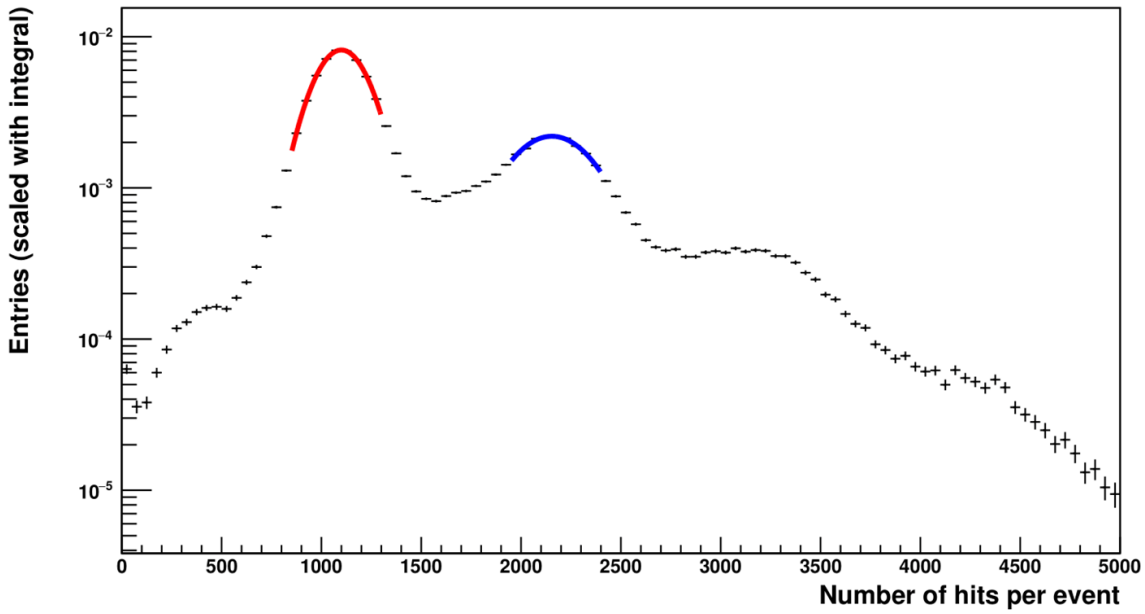

Figure 35: Run 1345

5 GeV runs

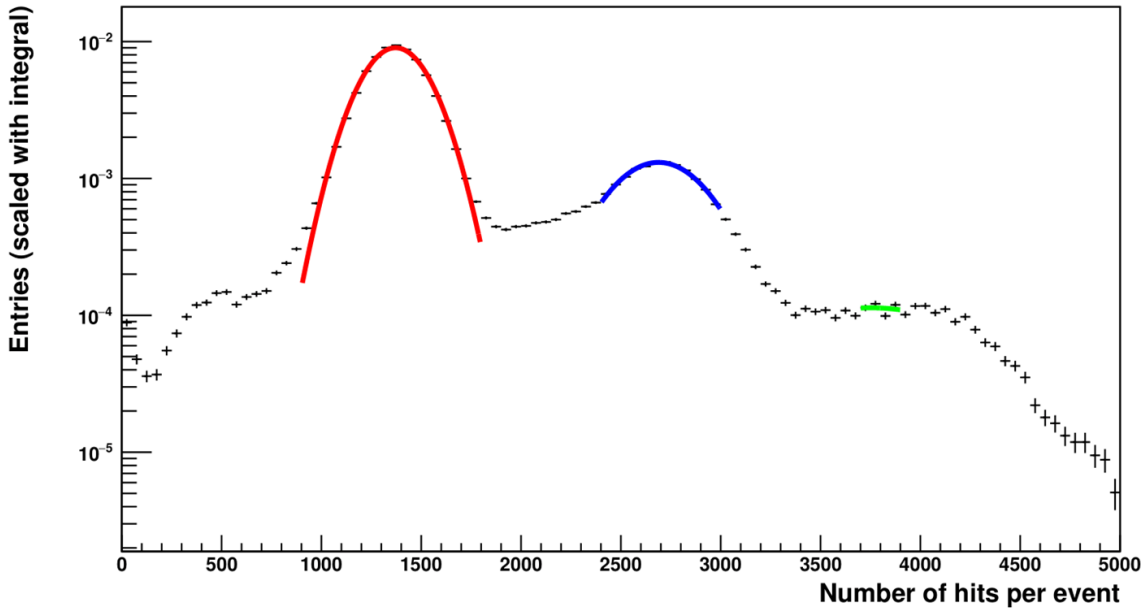

Figure 36: Run 1261

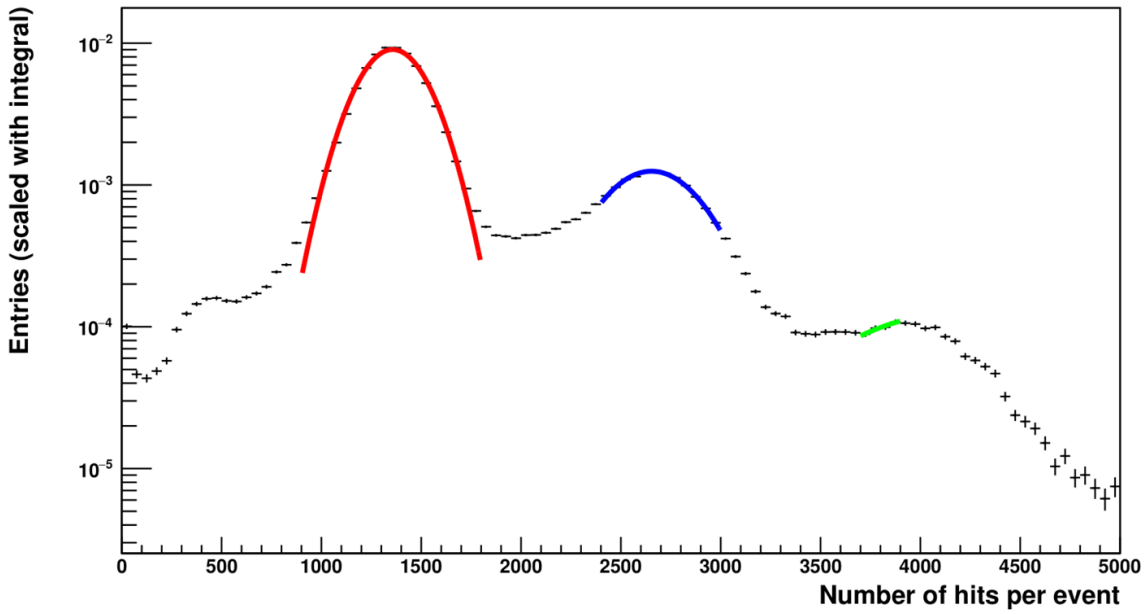

Figure 37: Run 1333

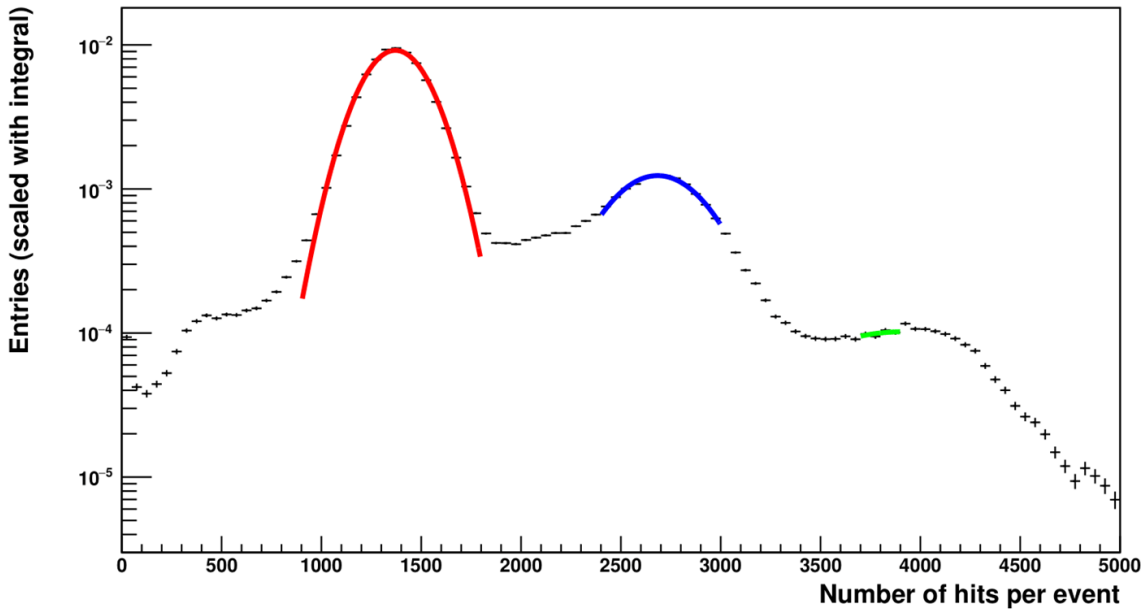

Figure 38: Run 1339

5.8 GeV runs

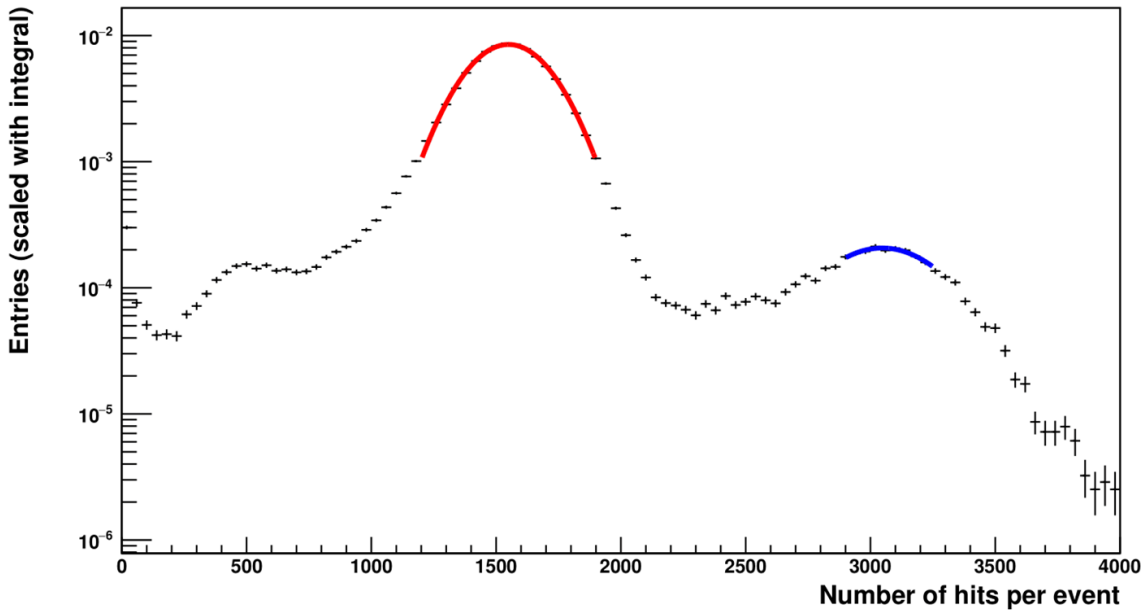

Figure 39: Run 1310

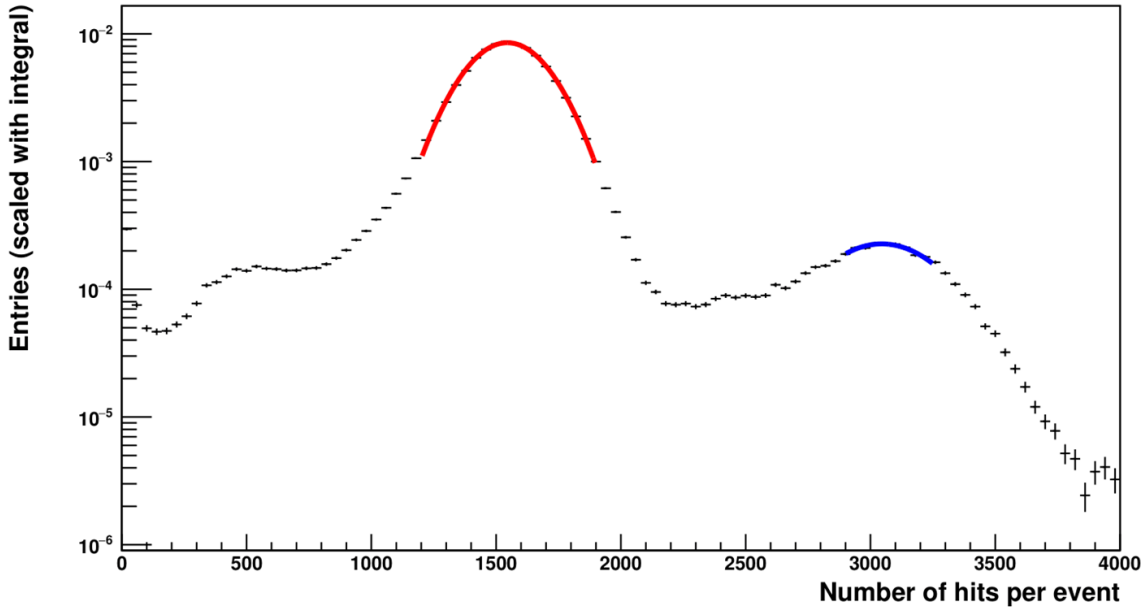

Figure 40: Run 1346